Miner Petrol (2017) 111:23–41
DOI 10.1007/s00710-016-0461-3

ORIGINAL PAPER

Petrogenesis of granitoids in the eastern section of the Central Qilian Block: Evidence from geochemistry and zircon U-Pb geochronology

Jiyong Li[1,2,3] · Yaoling Niu[1,2,4] · Shuo Chen[1,2,3] · Wenli Sun[1] · Yu Zhang[6] · Yi Liu[5] · Yuxin Ma[6] · Zhenxing Hu[6] · Guorui Zhang[6]

Received: 16 February 2016 / Accepted: 1 August 2016 / Published online: 10 August 2016

Abstract The Caledonian-age Qilian Orogenic Belt at the northern margin of the Greater Tibetan Plateau comprises abundant granitoids that record the histories of the orogenesis. We report here our study of these granitoids from two localities. The Qingchengshan (QCS) pluton, which is situated in the eastern section of the Central Qilian Block, is dated at ~430–420 Ma. It has high-K calc-alkaline composition with high SiO_2 (> 70 wt%), enrichment in large ion lithophile elements (LILEs), depletion in high field strength elements (HFSEs), and varying degrees of negative Sr and Eu anomalies. The granitoids in the Tongwei (TW) area, 150 km east of the QCS, are complex, the majority of which are dated at ~440 Ma, but there also exist younger, ~230 Ma intrusions genetically associated with the Qinling Orogeny. The Paleozoic TW intrusions also have high SiO_2, fractionated REE (rare earth element) patterns, but a negligible Eu anomaly. The whole rock Sr-Nd-Hf isotopic compositions suggest that all these Paleozoic granitoids are consistent with melting-induced mixing of a two-component source, which is best interpreted as the combination of last fragments of subducted/subducting ocean crust with terrigenous sediments. The mantle isotopic signature of these granitoids ($^{87}Sr/^{86}Sr_i$: 0.7038 to 0.7100, $\varepsilon_{Nd}(t)$: −4.8 to −1.3, $\varepsilon_{Hf}(t)$: −0.7 to +4.0) reflects significant (~70 %) contribution of the ocean crust derived in no distant past from the mantle at ocean ridges with an inherited mantle isotopic signature. Partial melting of such ocean crust plus terrigenous sediments in response to the ocean closing and continental collision (between the Qilian and Alashan Blocks) under amphibolite facies conditions is responsible for the magmatism. Varying extents of fractional crystallization (±plagioclase, ±amphibole, ±garnet, ±zircon) of the parental magmas produced the observed QCS and TW granitoids. We note that sample HTC12–01 in the TW area shows an A-type or highly fractionated granite signature characterized by elevated abundances and a flat pattern of REEs, weak Nb-Ta anomaly, conspicuous negative Sr and Eu anomalies (Sr/Sr* = 0.09, Eu/Eu* = 0.22), and thus the high $^{87}Sr/^{86}Sr$ ratio (0.7851), and moderate $\varepsilon_{Nd}(t)$ (−4.9) and $\varepsilon_{Hf}(t)$ (−2.0), pointing to the significant mantle contribution. Compared with the Paleozoic granitoids, the ~230 Ma granitoids in the TW area represented by sample JPC12–02 have higher initial $^{87}Sr/^{86}Sr$ (0.7073) and lower $\varepsilon_{Nd}(t)$ (−6.2) and $\varepsilon_{Hf}(t)$ (−4.5) values, offering an ideal opportunity for future studies on tectonic effects of juxtaposition of younger orogenesis on an older orogen.

Keywords Granitoids · Central Qilian Block · Ocean crust · Continental collision

Editorial handling: Y. Xu

✉ Jiyong Li
lijiy09@163.com

✉ Yaoling Niu
yaoling.niu@foxmail.com

[1] Present address: Institute of Oceanology, Chinese Academy of Sciences, No. 7 Nanhai Road, Qingdao 266071, China

[2] Laboratory for Marine Geology, Qingdao National Laboratory for Marine Science and Technology, Qingdao 266061, China

[3] University of Chinese Academy of Sciences, Beijing 100049, China

[4] Department of Earth Sciences, Durham University, Durham DH1 3LE, UK

[5] School of Earth Sciences and Resources, China University of Geosciences, Beijing 100083, China

[6] School of Earth Sciences, Lanzhou University, Lanzhou 730000, China

Introduction

Granitoids are abundant in all the orogenic belts worldwide. They are commonly classified as I-, S-, or A-types on the basis of their source rocks or compositional characteristics (Bonin 2007; Breiter et al. 2014; Champion and Bultitude 2013; Chappell 1999; Chappell and White 1992; Clemens et al. 2011). Recent studies have shown that the petrogenesis of granitoids are complex and cannot be described in terms of the above simple classification. Many granitoids in orogenic belts show characteristics of source or melt mixing (Gray and Kemp 2009; Peng et al. 2015; Xia et al. 2014; Yang et al. 2015; Zhu et al. 2015). Hence, classification of the petrogenesis of granitoids and using their geochemistry to indicate tectonic settings must be exercised with caution.

The Qilian Orogenic Belt (QOB) is a subduction-accretionary orogenic belt, which occupies an important position at the northern margin of the Greater Tibetan Plateau. The QOB records the histories of the collisional orogenesis, but how to correctly read the histories of the QOB remains controversial (Gehrels et al. 2003a; Huang et al. 2015; Song et al. 2013, 2014; Wu et al. 2006b, 2010; Xiao et al. 2009; Yang et al. 2015).

In this paper, we focus on the tectonically important yet poorly studied granitoids in the eastern section of the Central Qilian Block, located in the conjunction of the Qilian and Qinling Orogenic Belts, which is thus of particular tectonic significance. We present age data, major and trace element analysis and Sr-Nd-Hf isotope compositions to place constraints on the petrogenesis of these granitoids in the Central Qilian Block in the context of the tectonic evolution of the QOB.

Geological setting and petrography

The QOB is bounded by the North Qaidam Ultra-High-Pressure Metamorphic (UHPM) Belt and West-Qinling Orogenic Belt to the south, by the Alashan Block to the north, and is offset by the Altyn-Tagh Fault to the northwest (Fig. 1a) (Pan et al. 2009). Debate remains on the tectonic division of the QOB. The most recent suggested subdivisions from north to south are as follows (Fig. 1b): (1) The North Qilian Orogenic Belt (NQOB), thought to have resulted from the closure of the North Qilian Ocean, is characterized by arc volcanic rocks, exhumed high-pressure metamorphic rocks (Song et al. 2009a; Xia et al. 2012; Xiao et al. 2013; Zhang et al. 2009), and ophiolite sequences (Hou et al. 2006a; Shi et al. 2004; Xia and Song 2010; Zhang et al. 2003); (2) The Central Qilian Block (CQB), considered as an arc-accretionary system, is dominated by Precambrian basement overlain by the Paleozoic sedimentary lithologies (Tung et al. 2012; Xiao et al. 2009; Xu et al. 2010a, b), as well as the synchronous granitoids, granitic gneisses, amphibolites and minor granulites (Huang et al. 2015; Song et al. 2013, 2014). Recent studies suggest that the Central Qilian Block and Qaidam Block have close affinities with the Yangtze Craton (Darby and Gehrels 2006; Gehrels et al. 2003b; Tung et al. 2012; Xu et al. 2015), but this is debatable (Huang et al. 2015). Furthermore, the subdivision of the South Qilian Orogenic Belt (dotted line in Fig. 1b) composed of volcanic rocks and limestones (Xiao et al. 2009) on the basis of limited study, is also questionable; (3) The North Qaidam UHPM Belt is dominated by granitic and pelitic gneisses with eclogite lenses. Previous studies indicate that the North Qaidam UHPM Belt has experienced the processes from continental deep subduction to subsequent exhumation (Liu et al. 2012; Song et al. 2009b, 2014; Zhang et al. 2010); (4) The Qaidam Block (QDB), has a Precambrian meta-crystalline basement overlain by the Paleozoic-Mesozoic sedimentary strata (Song et al. 2013, 2014).

The Proterozoic strata in our study area in the eastern section of the CQB mainly contain the Huangyuan Group, Maxianshan Group, Xinglongshan Group and Gaolan Group, most of which are covered by Mesozoic-Cenozoic strata (Guo et al. 1999). The main intrusive rocks are Qingchengshan (QCS) Early Paleozoic biotite monzogranites intruding the Mesoproterozoic Gaolan Group (Fig. 1c) (Chen et al. 2008). Chen et al. (2008) reported two groups of zircon U-Pb ages for the QCS pluton (444 ± 3 Ma and 414 ± 3 Ma), and interpreted the former age as representing the emplacement of the pluton and the latter age as somewhat ambiguous thermal overprint. From the QCS pluton eastward, the synchronous Early Paleozoic calc-alkaline granitoids which intruded the Early Silurian Huluhe Group are also exposed in the Tongwei (TW) area spatially coexisting with minor Early Mesozoic plutons outcropped in the gullies as previously documented (Fig. 1d) (Zhang et al. 2005b), but they are essentially unstudied.

We have collected fresh samples from the QCS pluton and in the TW area (Fig. 2). The QCS pluton is compositionally biotite monzogranite dominated by plagioclase (30 ~ 40 vol.%), K-feldspar (30 ~ 40 vol.%), quartz (30 ~ 35 vol.%), biotite (5 ~ 10 vol.%) and minor accessory minerals such as zircon and magnetite. The granitoids in the TW area are mainly monzogranites and biotite granites, composed of K-feldspar (20 ~ 25 vol.%), plagioclase (35 ~ 40 vol.%) quartz (30 ~ 35 vol.%), and biotite (< 5 vol.%) with minor accessory minerals such as titanite and zoisite.

Analytical methods

We selected 4 samples (QCS12–07; QCS12–10; ABYC12–01; JPC12–02) for zircon U-Pb dating and 9 samples for whole-rock major and trace element analysis. All of them were analyzed for Sr-Nd-Hf isotopes.

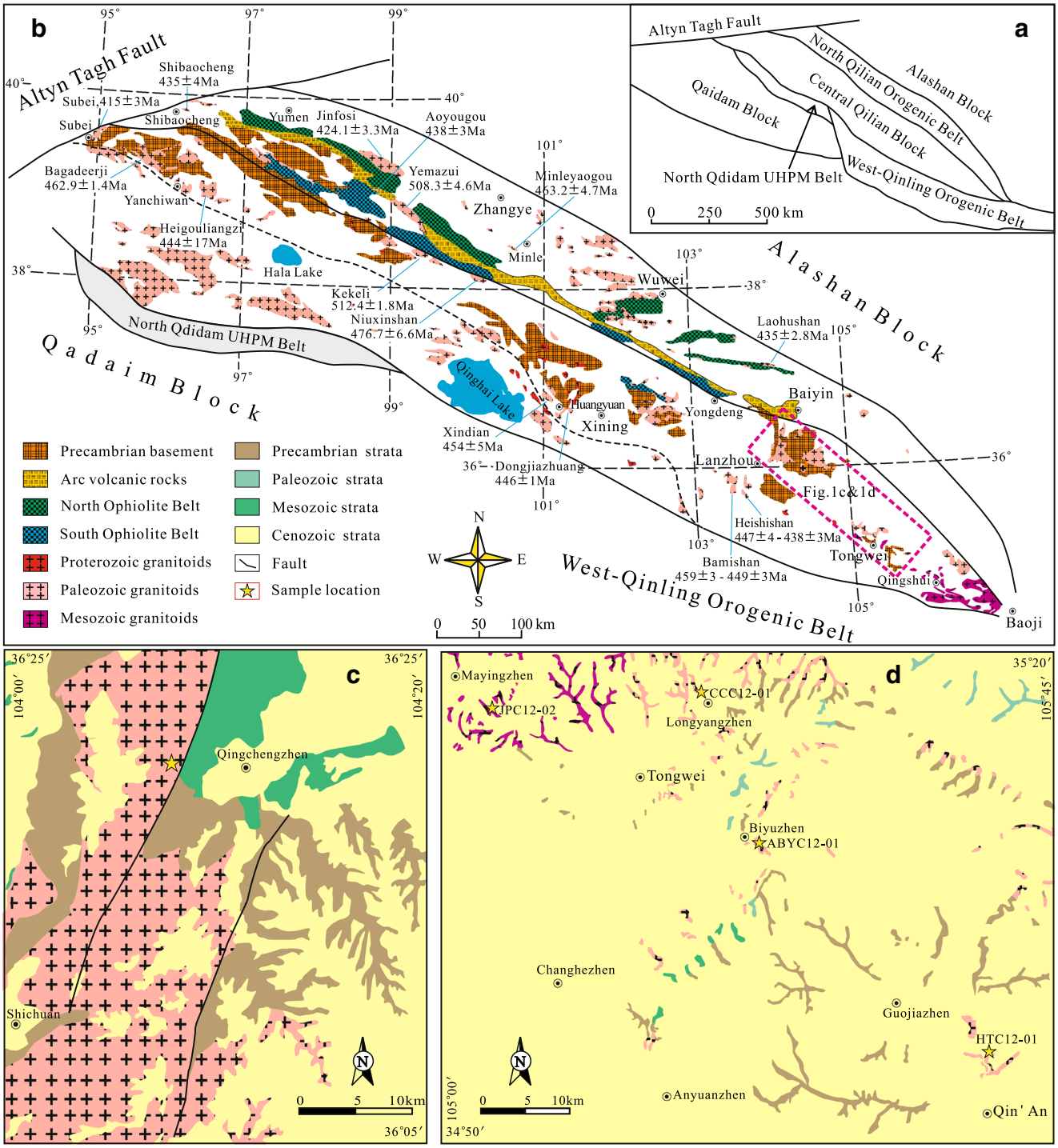

Fig. 1 **a** Schematic map showing major tectonic units of the Qilian Orogenic Belt and its adjacent areas (after Huang et al. 2015). **b** Simplified geological map showing the distribution of granitoids of varying age in the Qilian Orogenic Belt (modified from Ma et al. 2001 and Song et al. 2013). **c** Geological map of the Qingchengshan (QCS) pluton and **d** Geological map of the Tongwei (TW) area showing the location of granitoid outcrops with sampling sites. The zircon U-Pb age data in **b** are from Qian et al. (1998); Su et al. (2004); Wu et al. (2006b, 2010); Yong et al. (2008); Li et al. (2010); Chen et al. (2012); Qi (2012), and Yang et al. (2015)

Zircon U-Pb isotopic dating

Zircon separation was done using combined methods of heavy liquid and magnetic extraction plus hand-picking under a binocular in the Langfang Institute of Regional Geological Survey. The selected zircon grains were mounted in an epoxy resin disk and polished to expose the interior for imaging and analysis. All the polished zircon grains were examined using

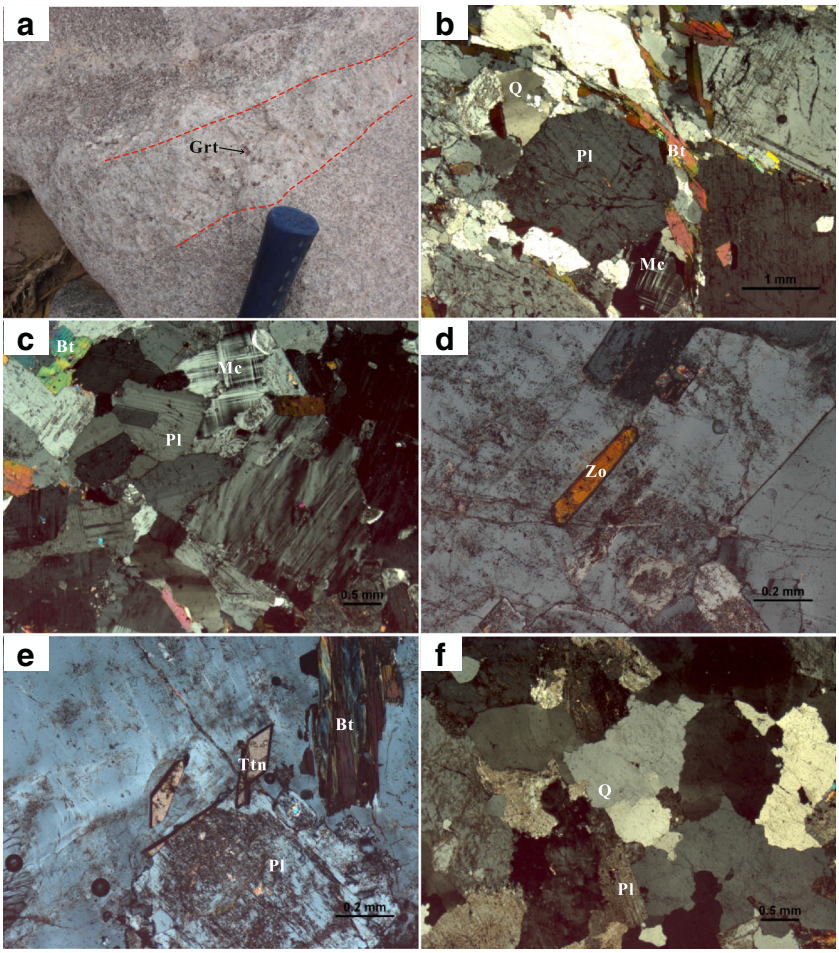

Fig. 2 **a** Field photograph showing garnet crystals in a pegmatite vein in the Qingchengshan (QCS) pluton. **b** Representative photomicrograph showing the mineral assemblages of the Qingchengshan pluton (QCS12–10). **c**, **d**, **e** and **f** are photomicrographs of other samples (ABYC12–01, JPC12–02, CCC12–01, HTC12–01) in the Tongwei (TW) area, respectively. Mineral abbreviations: Bt-biotite, Pl-plagioclase, Q-quartz, Ttn-titanite, Mc-microcline, Zo-zoisite

cathodoluminescence (CL) images at China University of Geosciences in Wuhan (CUGW). Zircon U-Pb dating was done using LA-ICP-MS at China University of Geosciences in Beijing (CUGB). Detailed analytical procedures are given in Song et al. (2010a). The data reduction was done using Glitter 4.4.1, followed by common Pb correction according to Andersen (2002). The weighted mean age calculations and concordia diagrams were done using isoplot 3.0 (Ludwig 2003).

Whole rock major and trace element analysis

The whole-rock major and trace element analysis was done at CUGB, using Leeman Prodigy inductively coupled plasma-optical emission spectroscopy (ICP-OES) and Agilent-7500a inductively coupled plasma mass spectrometry (ICP-MS), respectively. The analytical uncertainties are generally less than 1 % for most major elements with the exception of TiO_2 (~1.5 %) and P_2O_5 (~2 %). The loss on ignition was measured

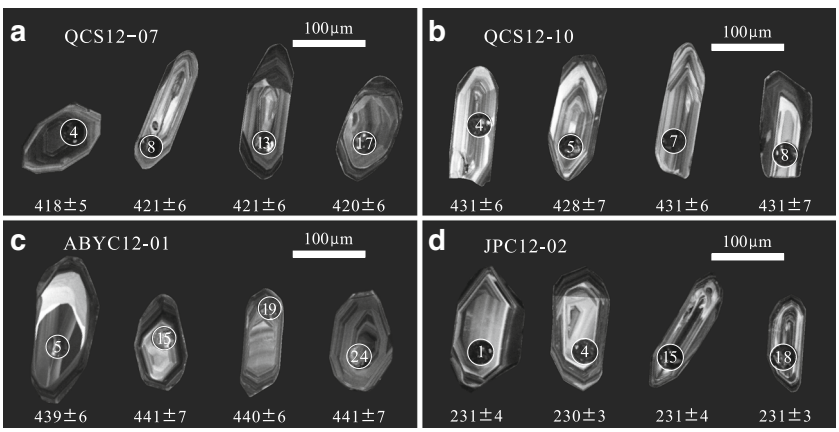

Fig. 3 Cathodoluminescence (CL) images of representative zircons for the Qingchengshan (QCS) pluton (QCS12–07, QCS12–10) and Tongwei (TW) granitoids (ABYC12–01, JPC12–02). Small solid circles are spots for U-Pb isotope analysis

Table 1 Zircon LA-ICP-MS U-Pb isotopic data of the Qingchengshan (QCS) pluton (QCS12–07, QCS12–10) and Tongwei (TW) granitoids (ABYC12–01, JPC12–02)

Grain-Spot	Th (ppm)	U (ppm)	Th/U	Ratios						Age (Ma)					
				$^{207}Pb/^{206}Pb$	± 1	$^{207}Pb/^{235}U$	**± 1**	$^{206}Pb/^{238}U$	**± 1**	$^{207}Pb/^{206}Pb$	± 1	$^{207}Pb/^{235}U$	± 1	$^{206}Pb/^{238}U$	± 1
QCS12–07															
1	345	452	0.76	0.0552	0.0027	0.5134	0.0238	0.0675	0.0010	419	111	421	16	421	6
2	297	606	0.49	0.0545	0.0010	0.5067	0.0096	0.0674	0.0009	393	21	416	6	420	5
3	112	247	0.45	0.0545	0.0015	0.5058	0.0137	0.0673	0.0010	393	36	416	9	420	6
4	110	624	0.18	0.0556	0.0010	0.5145	0.0101	0.0671	0.0009	438	22	421	7	418	5
5	130	272	0.48	0.0558	0.0013	0.5176	0.0126	0.0673	0.0010	445	30	424	8	420	6
6	148	260	0.57	0.0553	0.0015	0.5133	0.0145	0.0673	0.0010	424	38	421	10	420	6
7	124	283	0.44	0.0574	0.0015	0.5342	0.0139	0.0675	0.0010	507	33	435	9	421	6
8	125	361	0.35	0.0552	0.0012	0.5140	0.0115	0.0675	0.0009	422	26	421	8	421	6
9	138	436	0.32	0.0555	0.0012	0.5141	0.0114	0.0672	0.0009	430	26	421	8	419	6
10	332	821	0.40	0.0546	0.0009	0.5071	0.0092	0.0673	0.0009	397	19	416	6	420	5
11	347	540	0.64	0.0551	0.0011	0.5123	0.0110	0.0674	0.0009	416	25	420	7	421	6
12	82.2	168	0.49	0.0561	0.0020	0.5219	0.0183	0.0674	0.0010	458	51	426	12	421	6
13	110	415	0.26	0.0558	0.0012	0.5193	0.0115	0.0675	0.0009	446	26	425	8	421	6
14	126	229	0.55	0.0562	0.0015	0.5217	0.0143	0.0673	0.0010	460	36	426	10	420	6
15	159	340	0.47	0.0541	0.0011	0.5015	0.0108	0.0673	0.0009	374	25	413	7	420	6
16	208	284	0.73	0.0553	0.0013	0.5134	0.0127	0.0674	0.0010	422	31	421	9	420	6
17	114	581	0.20	0.0556	0.0011	0.5165	0.0106	0.0674	0.0009	436	23	423	7	420	6
18	106	178	0.60	0.0558	0.0018	0.5199	0.0166	0.0676	0.0010	445	44	425	11	421	6
19	166	252	0.66	0.0553	0.0015	0.5136	0.0145	0.0673	0.0010	425	37	421	10	420	6
20	139	314	0.44	0.0552	0.0021	0.5136	0.0194	0.0674	0.0011	422	55	421	13	421	7
21	270	351	0.77	0.0548	0.0012	0.5110	0.0118	0.0676	0.0010	406	27	419	8	422	6
22	217	380	0.57	0.0547	0.0012	0.5069	0.0119	0.0672	0.0010	400	28	416	8	419	6
QCS12–10															
1	161	265	0.61	0.0552	0.0015	0.5251	0.0147	0.0690	0.0010	420	36	429	10	430	6
2	168	314	0.53	0.0565	0.0028	0.5329	0.0251	0.0684	0.0011	472	113	434	17	427	6
3	162	284	0.57	0.0555	0.0014	0.5286	0.0141	0.0691	0.0010	431	34	431	9	431	6
4	126	221	0.57	0.0553	0.0019	0.5273	0.0181	0.0692	0.0011	424	49	430	12	431	6
5	196	369	0.53	0.0556	0.0019	0.5265	0.0179	0.0687	0.0011	436	48	429	12	428	7
6	107	193	0.56	0.0554	0.0020	0.5289	0.0188	0.0692	0.0012	429	50	431	13	431	7
7	146	356	0.41	0.0560	0.0016	0.5339	0.0155	0.0691	0.0010	454	38	434	10	431	6
8	218	282	0.77	0.0556	0.0019	0.5298	0.0178	0.0691	0.0011	437	46	432	12	431	7
9	178	284	0.63	0.0555	0.0016	0.5272	0.0158	0.0689	0.0011	432	40	430	10	430	6
ABYC12–01															
1	156	190	0.82	0.0562	0.0016	0.5482	0.0156	0.0707	0.0011	460	37	444	10	441	6
2	244	334	0.73	0.0565	0.0014	0.5508	0.0141	0.0707	0.0010	471	31	446	9	441	6
3	200	296	0.68	0.0557	0.0014	0.5419	0.0145	0.0706	0.0010	440	34	440	10	440	6
4	278	215	1.29	0.0563	0.0017	0.5476	0.0170	0.0705	0.0011	465	42	443	11	439	7
5	278	334	0.83	0.0555	0.0014	0.5401	0.0139	0.0705	0.0010	434	32	439	9	439	6
6	71.8	109	0.66	0.0555	0.0026	0.5416	0.0254	0.0708	0.0012	432	75	439	17	441	7
7	231	227	1.02	0.0556	0.0016	0.5416	0.0158	0.0707	0.0011	435	38	439	10	440	7
8	303	255	1.19	0.0550	0.0016	0.5352	0.0155	0.0706	0.0011	411	38	435	10	440	6
9	243	422	0.58	0.0554	0.0012	0.5412	0.0126	0.0708	0.0010	430	27	439	8	441	6
10	198	285	0.70	0.0563	0.0014	0.5475	0.0140	0.0705	0.0011	464	31	443	9	439	6
11	234	273	0.86	0.0557	0.0016	0.5436	0.0156	0.0708	0.0011	440	37	441	10	441	6
12	219	344	0.64	0.0554	0.0013	0.5391	0.0130	0.0705	0.0010	430	29	438	9	439	6

Table 1 (continued)

Grain-Spot	Th (ppm)	U (ppm)	Th/U	Ratios						Age (Ma)					
				$^{207}Pb/^{206}Pb$	± 1	$^{207}Pb/^{235}U$	**± 1**	$^{206}Pb/^{238}U$	**± 1**	$^{207}Pb/^{206}Pb$	± 1	$^{207}Pb/^{235}U$	± 1	$^{206}Pb/^{238}U$	± 1
13	126	127	1.00	0.0565	0.0022	0.5519	0.0214	0.0709	0.0011	471	57	446	14	441	7
14	828	726	1.14	0.0587	0.0012	0.5696	0.0121	0.0703	0.0010	557	23	458	8	438	6
15	132	147	0.90	0.0557	0.0020	0.5438	0.0198	0.0708	0.0011	441	53	441	13	441	7
16	119	234	0.51	0.0584	0.0016	0.5843	0.0161	0.0725	0.0011	546	34	467	10	451	7
17	125	297	0.42	0.0553	0.0012	0.5392	0.0124	0.0707	0.0010	424	27	438	8	440	6
18	313	480	0.65	0.0564	0.0011	0.5495	0.0116	0.0707	0.0010	468	23	445	8	440	6
19	547	658	0.83	0.0552	0.0011	0.5385	0.0112	0.0707	0.0010	422	23	437	7	440	6
20	385	493	0.78	0.0553	0.0011	0.5407	0.0117	0.0709	0.0010	426	25	439	8	441	6
21	192	185	1.04	0.0555	0.0016	0.5411	0.0158	0.0708	0.0011	430	38	439	10	441	7
22	448	271	1.65	0.0600	0.0015	0.5827	0.0147	0.0705	0.0011	602	30	466	9	439	6
23	64.5	115	0.56	0.0554	0.0022	0.5413	0.0215	0.0708	0.0011	430	61	439	14	441	7
24	84.0	136	0.62	0.0537	0.0020	0.5249	0.0197	0.0709	0.0011	359	56	428	13	441	7
JPC12–02															
1	111	281	0.40	0.0503	0.0020	0.2528	0.0099	0.0364	0.0006	211	61	229	8	231	4
2	68.6	124	0.55	0.0513	0.0031	0.2576	0.0153	0.0364	0.0006	254	106	233	12	231	4
3	328	239	1.37	0.0509	0.0017	0.2561	0.0087	0.0365	0.0006	235	50	232	7	231	3
4	310	498	0.62	0.0507	0.0015	0.2542	0.0075	0.0363	0.0006	229	41	230	6	230	3
5	380	256	1.49	0.0508	0.0023	0.2551	0.0116	0.0365	0.0006	230	75	231	9	231	4
6	154	226	0.68	0.0511	0.0024	0.2567	0.0118	0.0364	0.0006	245	76	232	10	231	4
7	444	261	1.70	0.0508	0.0019	0.2554	0.0096	0.0365	0.0006	232	59	231	8	231	3
8	286	185	1.55	0.0504	0.0028	0.2517	0.0138	0.0362	0.0006	214	96	228	11	229	4
9	327	295	1.11	0.0507	0.0022	0.2518	0.0107	0.0360	0.0006	228	70	228	9	228	3
10	97.3	352	0.28	0.0510	0.0013	0.2561	0.0066	0.0365	0.0005	239	33	232	5	231	3
11	279	207	1.35	0.0509	0.0022	0.2563	0.0111	0.0366	0.0006	234	71	232	9	231	4
12	178	311	0.57	0.0507	0.0016	0.2548	0.0081	0.0364	0.0005	228	46	230	7	231	3
13	313	541	0.58	0.0528	0.0031	0.2560	0.0142	0.0351	0.0006	322	134	231	11	223	3
14	374	930	0.40	0.0508	0.0011	0.2558	0.0058	0.0365	0.0005	230	28	231	5	231	3
15	575	303	1.90	0.0506	0.0019	0.2547	0.0095	0.0365	0.0006	224	57	230	8	231	4
16	103	80	1.28	0.0506	0.0046	0.2516	0.0224	0.0361	0.0008	221	159	228	18	229	5
17	123	118	1.04	0.0512	0.0038	0.2514	0.0187	0.0356	0.0007	252	135	228	15	225	4
18	568	535	1.06	0.0527	0.0014	0.2651	0.0074	0.0365	0.0005	316	38	239	6	231	3
19	74.5	240	0.31	0.0511	0.0023	0.2565	0.0116	0.0364	0.0006	244	73	232	9	231	4

by placing 1 g of sample powder in the furnace at 1000 °C for several hours before cooled in a desiccator and reweighted. The Analytical details are given in Song et al. (2010b).

Sr-Nd-Hf isotope analysis

The Sr-Nd-Hf isotope analysis was done at Guangzhou Institute of Geochemistry, Chinese Academy of Sciences (GIG-CAS), following the methods by Li et al. (2006). The rock powders were dissolved with HF-HNO_3 mixtures before Sr, Nd and Hf separation by small Sr Spec resin columns and Hf-Nd cation exchange resin columns to obtain purified Sr, Nd and Hf fractions. The Sr isotope analysis was done using a Neptune Plus multi-collector inductively coupled plasma mass spectrometer (MC-ICP-MS), and Nd-Hf isotope analyses were done using a Micromass IsoProbe MC-ICP-MS. All measured $^{87}Sr/^{86}Sr$, $^{143}Nd/^{144}Nd$ and $^{176}Hf/^{177}Hf$ ratios were normalized to $^{86}Sr/^{88}Sr = 0.1194$, $^{146}Nd/^{144}Nd = 0.7219$ and $^{179}Hf/^{177}Hf = 0.7325$, respectively. During the course of this study, analyses of NBS987 standard gave $^{87}Sr/^{86}Sr = 0.710283 \pm 0.000005$ ($n = 13$, 2σ). The $^{143}Nd/^{144}Nd$ ratios of the standard BHVO-2 and JB-3 were 0.512977 ± 0.000014 ($n = 8$, 2σ) and 0.513053 ± 0.000018 ($n = 13$, 2σ), respectively. And the mean $^{176}Hf/^{177}Hf$ ratios for

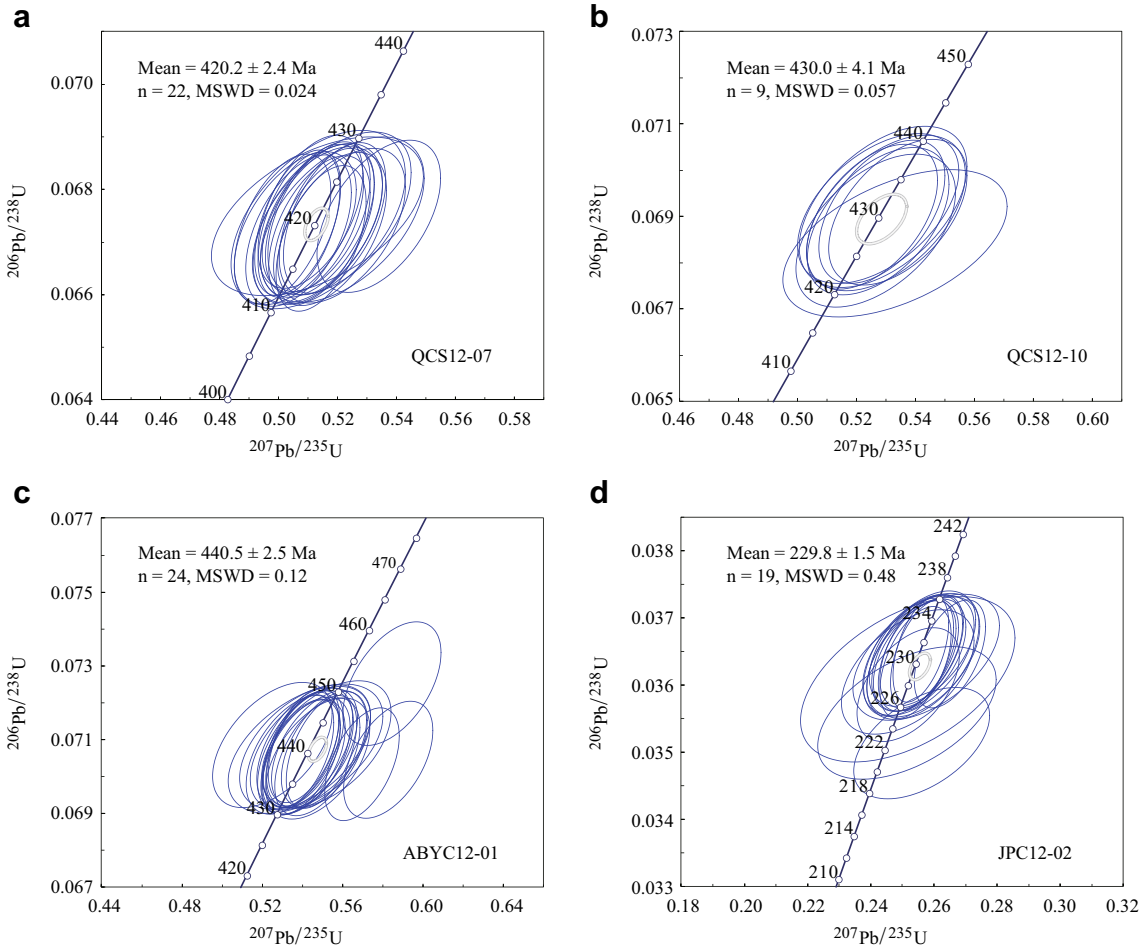

Fig. 4 Concordia diagrams of U-Pb zircon ages for the Qingchengshan (QCS) pluton (QCS12–07, QCS12–10) and Tongwei (TW) granitoids (ABYC12–01, JPC12–02)

BHVO-2 and JB-3 were 0.283099 ± 0.000015 (n = 13, 2σ) and 0.283216 ± 0.000015 (*n* = 6, 2σ), respectively. The values of rock standards BHVO-2 and JB-3 are within the analytical error of the recommended values (GeoREM, http://georem.mpch-mainz.gwdg.de/).

Analytical data

Zircon U-Pb geochronology

Representative zircon Cathodoluminescence (CL) images for the QCS pluton and TW granitoids are shown in Fig. 3. LA-ICP-MS zircon U-Pb data are given in Table 1 and presented in Fig. 4.

Zircons in sample QCS12–07 (from the QCS pluton) are euhedral and elongated crystals with oscillatory-zoning of magmatic origin (Fig. 3a), having variably high Th/U (0.18–0.77). Twenty two analyses yield a weighted mean $^{206}Pb/^{238}U$ age of 420.2 ± 2.4 Ma (MSWD =0.024) (Fig. 4a). Nine analyses of zircons in sample QCS12–10 (from the QCS pluton) with high Th/U (0.41–0.77) give a weighted mean $^{206}Pb/^{238}U$ age of 430.0 ± 4.1 Ma (MSWD =0.057) (Fig. 4b).

Zircons in sample ABYC12–01 (from the TW granitoids) show variable Th/U (0.42–1.65), and twenty four analyses of zircons give a weighted mean $^{206}Pb/^{238}U$ age of 440.5 ± 2.5 Ma (MSWD =0.12) (Fig. 4c). Nineteen analyses of zircons in sample JPC12–02 (from the TW granitodis) show varying Th/U values (0.31–1.90) and oscillatory zoning (Fig. 3d), yielding a weighted mean $^{206}Pb/^{238}U$ age of 229.8 ± 1.5 Ma (MSWD =0.48) (Fig. 4d).

Whole-rock major and trace element data

Whole-rock major and trace element data of 9 samples (5 QCS samples, 4 TW samples) are given in Table 2.

All the QCS samples show high SiO_2 (70.6–75.7 wt%) and relatively high alkalis (K_2O + Na_2O = 6.4–7.8 wt%). These data plot in the granite field in the TAS diagram (Fig. 5a). Most of the samples display high-K calc-alkaline (Fig. 5b) and metaluminous to peraluminous (A/CNK = 0.99–1.12)

Table 2 Whole-rock major and trace element data of the Qingchengshan (QCS) pluton and Tongwei (TW) granitoids

Sample	QCS pluton					TW granitoids			
	QCS12–03	QCS12–06	QCS12–08	QCS12–10	QCS12–11	JPC12–02	CCC12–01	ABYC12–01	HTC12–01
SiO_2	73.8	70.6	72.5	70.8	75.7	71.8	71.6	70.8	74.7
TiO_2	0.14	0.26	0.25	0.35	0.07	0.31	0.26	0.32	0.21
Al_2O_3	13.8	15.4	14.9	14.7	14.3	14.7	14.6	14.9	13.0
TFe_2O_3 [a]	1.19	2.02	2.02	2.46	0.49	2.04	1.73	2.21	1.25
MnO	0.06	0.04	0.03	0.03	0.01	0.03	0.03	0.03	0.01
MgO	0.24	0.62	0.73	0.76	0.16	0.56	0.61	0.74	0.29
CaO	1.64	2.91	2.36	1.92	1.73	1.88	1.71	3.02	0.46
Na_2O	3.38	4.31	3.76	3.06	3.37	3.87	3.97	4.19	3.05
K_2O	4.42	3.01	2.62	4.54	3.83	4.30	4.29	2.93	5.36
P_2O_5	0.05	0.11	0.10	0.07	0.02	0.09	0.08	0.08	0.09
LOI	0.58	0.60	0.63	0.56	0.42	0.60	0.59	0.56	0.79
Total	99.2	99.9	99.9	99.2	100.0	100.2	99.5	99.8	99.1
A/NK [b]	1.33	1.49	1.65	1.48	1.47	1.33	1.31	1.49	1.20
A/NKC [c]	1.03	0.99	1.12	1.10	1.11	1.01	1.02	0.96	1.11
K_2O/Na_2O	1.31	0.70	0.70	1.48	1.35	1.11	1.08	0.70	1.76
Li	37.5	27.2	50.1	26.9	12.2	35.8	50.1	21.2	10.7
Sc	3.7	3.4	4.4	4.0	1.3	3.1	2.9	2.9	5.4
V	7.5	17.0	23.1	23.2	4.5	22.0	24.7	36.1	20.3
Cr	3.3	3.8	3.8	9.7	22.7	9.4	9.9	8.2	8.2
Co	0.6	2.4	2.9	3.6	0.8	2.5	2.6	3.8	1.1
Ni	0.8	1.7	2.8	4.5	10.8	4.6	5.1	4.4	1.7
Cu	2.3	1.1	5.5	1.6	0.8	5.3	3.6	2.2	57.0
Zn	29.0	35.7	49.7	46.8	14.2	40.1	31.5	42.1	14.2
Ga	18.1	18.4	19.7	18.9	16.5	19.8	20.6	21.8	18.9
Rb	181	105	162	116	129	165	210	105	344
Sr	101	337	342	379	317	534	599	907	63
Y	15.2	6.4	10.8	8.9	8.7	6.6	6.5	5.2	47.4
Zr	124	126	381	156	49	200	135	171	128
Nb	14.7	11.8	16.4	15.1	5.1	10.4	9.7	4.4	39.3
Cs	2.9	3.6	5.0	4.5	1.7	3.0	12.5	1.7	10.9
Ba	545	632	1555	739	758	1452	1209	1879	206
La	37.5	27.9	103.8	31.5	21.9	56.3	33.1	50.7	29.4
Ce	74.5	50.7	191.8	54.0	41.2	97.6	59.7	93.6	61.8
Pr	7.41	4.52	17.89	5.21	4.05	8.97	6.08	8.28	7.01
Nd	24.8	14.7	58.8	17.1	13.7	28.6	20.6	26.2	26.1
Sm	4.42	2.50	8.19	2.81	2.44	3.90	3.12	3.32	6.19
Eu	0.53	0.66	1.06	0.65	0.73	0.99	0.80	0.95	0.44
Gd	3.54	2.02	5.63	2.39	2.07	2.75	2.24	2.15	6.13
Tb	0.47	0.25	0.54	0.33	0.29	0.29	0.25	0.21	1.06
Dy	2.58	1.23	2.30	1.73	1.61	1.32	1.19	0.97	6.92
Ho	0.53	0.21	0.39	0.31	0.31	0.23	0.21	0.18	1.49
Er	1.71	0.58	1.06	0.84	0.82	0.63	0.60	0.51	4.79
Tm	0.28	0.08	0.13	0.11	0.10	0.08	0.08	0.07	0.74
Yb	1.97	0.48	0.77	0.65	0.61	0.50	0.53	0.50	5.26
Lu	0.29	0.07	0.12	0.09	0.09	0.08	0.08	0.08	0.78
Hf	3.24	3.22	8.78	3.74	1.39	4.52	3.43	3.94	3.89
Ta	0.93	0.96	0.89	0.98	0.34	0.66	0.60	0.27	2.95

Table 2 (continued)

Sample	QCS pluton					TW granitoids			
	QCS12–03	QCS12–06	QCS12–08	QCS12–10	QCS12–11	JPC12–02	CCC12–01	ABYC12–01	HTC12–01
Pb	26.9	30.1	32.7	25.9	32.8	31.2	38.4	19.4	41.8
Th	19.9	14.8	33.1	11.9	9.8	19.6	17.7	14.9	38.9
U	2.22	1.66	2.60	1.79	1.22	2.14	1.84	1.39	4.49
Eu/Eu* [d]	0.40	0.87	0.45	0.75	0.96	0.88	0.88	1.02	0.22
Sr/Sr* [d]	0.14	0.79	0.20	0.77	0.82	0.64	1.03	1.18	0.09
$(La/Yb)_N$ [e]	13.6	42.0	96.3	35.0	25.8	80.7	44.7	73.2	4.0
$(Dy/Yb)_N$ [e]	0.88	1.72	1.99	1.80	1.77	1.77	1.50	1.31	0.88

[a] Fe_2O_3 is total Fe expressed as Fe^{3+}

[b] A/NK = molar $Al_2O_3/(Na_2O + K_2O)$

[c] A/NKC = molar $Al_2O_3/(Na_2O + K_2O + CaO)$

[d] $Eu/Eu^* = 2 \times Eu_N/(Sm_N + Gd_N)$, $Sr/Sr^* = 2 \times Sr_N/(Pr_N + Nd_N)$

[e] Subscript $_N$ stands for normalized values against chondrite

characteristics (Fig. 5c). In SiO_2 variation diagrams (Fig. 6), most oxides do not exhibit well defined trends.

Trace elements of the QCS samples show enrichment of LILEs (Rb, K, Ba) and relative depletion of HFSEs (Nb, Ta, Ti, P) (Fig. 7a) with varying Nb/Ta ratios (12.3–18.4). Chondrite-normalized REE (rare earth element) patterns of these samples show varying enrichment of LREEs (light rare earth elements) ($[La/Yb]_N$ = 13.6–96.3) and variably fractionated HREEs (heavy rare earth elements) ($[Dy/Yb]_N$ = 0.88–1.99) (Fig. 7c). The samples also display variable negative Sr and Eu anomalies (Sr/Sr* = 0.14–0.82, Eu/Eu* = 0.40–0.96).

The ~440 Ma TW samples have high SiO_2 (70.8–74.7 wt%), and variable K_2O/Na_2O (0.70–1.76), plotting in the granite field in the TAS diagram (Fig. 5a) and displaying calc-alkaline to high-K calc-alkaline characteristics in the K_2O - SiO_2 diagram (Fig. 5b). They have relatively high A/CNK values (0.96–1.11) (Fig. 5c). Note that sample HTC12–01 has the highest SiO_2 (74.7 wt%) and lowest CaO (0.46 wt%). The ~230 Ma sample (JPC12–02) also shows high SiO_2 (71.8 wt%), high-K calc-alkaline (K_2O/Na_2O = 1.11) and metaluminous (A/CNK = 1.01) characteristics.

In model ocean crust normalized trace element diagram, the ~440 Ma TW samples show enrichment of LILEs (Rb, Ba, K) and depletion of HFSEs (Nb, Ta, Ti, P) (Fig. 7b). Most of these samples show elevated LREEs/HREEs ratios ($[La/Yb]_N$ = 44.7–73.2) without significant Sr and Eu anomalies (Sr/Sr* = 1.03–1.18, Eu/Eu* = 0.88–1.02), except for sample HTC12–01 which shows a flat HREE pattern, lower LREEs/HREEs ratio ($[La/Yb]_N$ = 4.0, $[Dy/Yb]_N$ = 0.88) and pronounced negative Sr and Eu anomalies (Sr/Sr* = 0.09, Eu/Eu* = 0.22). The ~230 Ma TW sample shows similar characteristics of trace element systematics with the ~440 Ma samples ($[La/Yb]_N$ = 80.7, Eu/Eu* = 0.88) (Fig. 7d).

Sr-Nd-Hf isotopes

The whole-rock Sr-Nd-Hf isotope data are given in Table 3.

The QCS samples show variable initial $^{87}Sr/^{86}Sr$ (0.7038 to 0.7100, calculated at 430 Ma), moderate $\varepsilon_{Nd}(t)$ (−4.8 to −1.3) and relatively high $\varepsilon_{Hf}(t)$ (−0.7 to +4.0) (Fig. 11). The mantle isotopic signature of the QCS samples reflects significant contribution to juvenile crustal growth. The ~440 Ma TW samples show relatively low initial $^{87}Sr/^{86}Sr$ (0.7038–0.7053), and high $\varepsilon_{Nd}(t)$ (−2.1 to −3.1) and $\varepsilon_{Hf}(t)$ values (+1.9 to +2.2) (Fig. 11), except for sample HTC12–01 with extremely high $^{87}Sr/^{86}Sr$ (0.7851, see below), while the ~230 Ma sample shows modest initial $^{87}Sr/^{86}Sr$ (0.7073), low $\varepsilon_{Nd}(t)$ (−6.2), and $\varepsilon_{Hf}(t)$ (−4.5).

Discussion

Petrogenesis of the QCS pluton

S-type granites or Adakite/Adakitic rocks?

A previous study (Chen et al. 2008) suggested that the QCS pluton is peraluminous S-type granites derived from partial melting of meta-greywackes in middle-upper crust conditions. However, there are no Al_2O_3-rich phases (e.g., cordierite, muscovite, garnet etc.) as would be expected for S-type granites. Garnet only appears as a vein mineral (Fig. 2a). As is the general case, S-type granites commonly contain enclaves representing restite of crustal melting (Chappell and White 1991; Chappell and Wyborn 2012), but such enclaves are

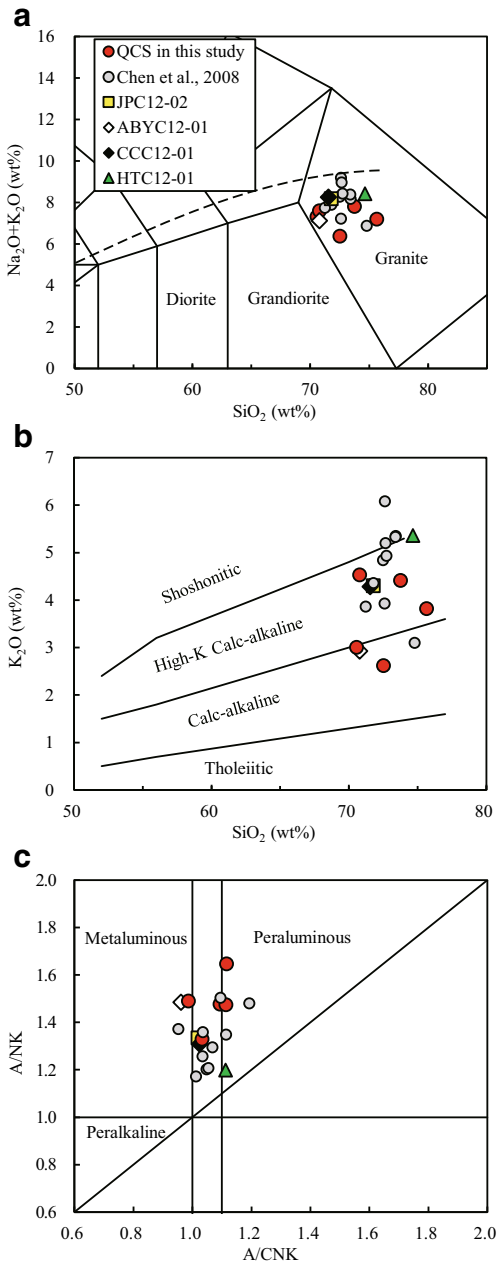

Fig. 5 **a** The total alkali vs. silica (TAS) diagram (after Middlemost 1994). **b** The K_2O vs. SiO_2 diagram (after Peccerillo and Taylor 1976) and **c** The A/NK vs. A/CNK diagram used for the classification of Qingchengshan (QCS) pluton and Tongwei (TW) granitoids. Red circles are our data in this study for the Qingchengshan pluton, and grey circles are the literature data for the Qingchengshan pluton (Chen et al. 2008). Other symbols are the samples from the Tongwei area (JPC12–02, ABYC12–01, HTC12–01, CCC12–01)

absent in the QCS pluton. In addition, the metaluminous to peraluminous characteristics (A/CNK = 0.99–1.12) and the roughly negative P_2O_5 - SiO_2 correlation (Fig. 6) which is used to distinguish I-type from S-type granites due to the high apatite solubility in peraluminous melt (Chappell 1999), suggest that the QCS pluton is not S-type granites derived from meta-sedimentary protolith.

Geochemically, although the QCS pluton has high Sr/Y (6.6–53.1) and La/Yb (19.0–134.2) ratios, it could be mistakenly interpreted as adakite or adakitic rocks. In Sr/Y vs. Y and La/Yb vs. Yb diagrams (Fig. 10a, b) which are commonly used to distinguish adakite from normal island arc rocks, our data and the data from the literature (Chen et al. 2008) plot cross the field of adakite and of normal arc andesite, dacite, and rhyolite (ADR). However, the QCS pluton has low Al_2O_3 (< 15 %), modest Sr (< 400 ppm) and low Y (< 20 ppm) and Yb (< 2 ppm). They are different from adakite and adakitic rocks by definition (e.g., high Sr > 400 ppm; Castillo 2012). Hence, the QCS pluton also cannot be defined as adakite or adakitic rocks.

High silica granites and high Sr/Y, La/Yb ratios

Note that the QCS pluton has high silica content (> 70 wt%) and the major element oxides (our data and literature data) do not show obvious evolution trend with SiO_2 (Fig. 6). It is likely that these high silica granites represent residual liquids with a felsic magmatic crystal mush (Lee and Morton 2015) at the late stage of magma evolution. As mentioned above, the QCS pluton shows high Sr/Y (6.6–53.1) and La/Yb (19.0–134.2) ratios. Additionally, the QCS pluton shows obvious enrichment of LREEs and depletion of HREEs relative to model bulk continental crust composition (BCC, Rudnick and Gao 2003) (Fig. 7c). It is thus important to evaluate the effect of fractional crystallization of relevant minerals phases (e.g., plagioclase, amphibole, zircon, garnet).

Firstly, fractional crystallization of plagioclase could play an important role in magma evolution as evidenced by decreasing Sr with increasing SiO_2 (Fig. 8a) and increasing Rb/Sr with decreasing Sr (Fig. 8b). Fractional crystallization of amphibole could cause high Sr/Y and La/Yb ratios, whereas the evolution trend with amphibole fractionation only in our simulation do not fit well with the data in Sr/Y vs. Y space (Fig. 10a, line2). Besides, amphibole fractionation will cause the residual melt to develop a concave HREE pattern (Moyen 2009), which is not observed (Fig. 7c). Crystallization of zircon is expected to deplete HREEs in the melt because of strong compatibility of HREEs in zircons (Thomas et al. 2002). Figure 9a shows that Zr/Sm indeed decreases with increasing SiO_2, which is consistent with zircon crystallization. However, Fig. 9b shows that zircon crystallization cannot explain the HREE depletion as approximated with Y. The relatively varying HREE fractionation (e.g., $[Dy/Yb]_N$ = 0.88–1.99) may be caused by garnet, which is highly compatible for the progressively heavier HREEs. Generally, garnet is regarded as a characteristic mineral of S-type granites, mainly formed by peritectic reaction during partial melting of pelites and psammites or other meta-sedimentary rocks (Sylvester 1998; Taylor and Stevens 2010). But in this study, garnet only appears as liquidus phase in veins (Fig. 2a) of late

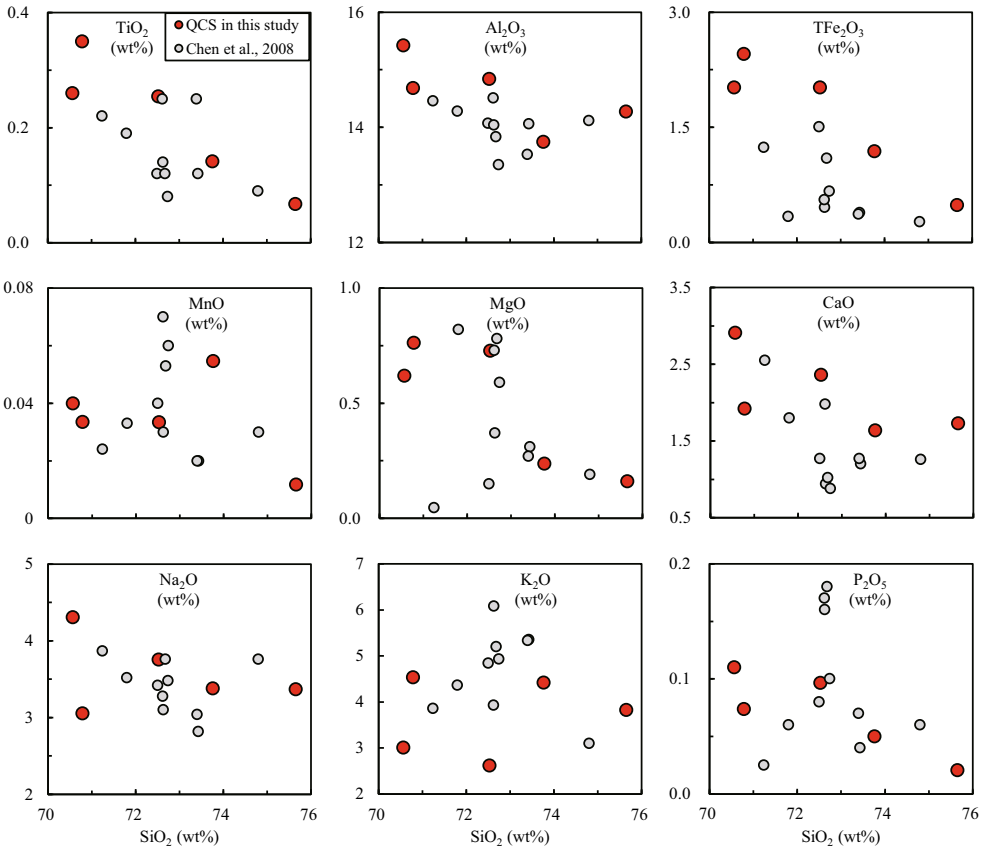

Fig. 6 SiO_2 variation diagrams for major element oxides on the Qingchenshan (QCS) pluton. Red circles are our new data, and grey circles are the literature data (Chen et al. 2008)

stage of magma evolution (Dahlquist et al. 2007; René and Stelling 2007). We thus suggest that the primitive magmas parental to the QCS pluton may have experienced fractional crystallization of garnet, resulting in HREE depletion.

With all the above considered, we carried out calculations shown in Fig. 10a, b, where the high Sr/Y and La/Yb ratios can be explained by fractional crystallization of garnet, plagioclase and amphibole.

Constraints on the source

The QCS pluton has varying initial $^{87}Sr/^{86}Sr$ (0.7038 to 0.7100) and moderate $\varepsilon_{Nd}(t)$ (−4.8 to −1.3) showing scattered but significant inverse trend falling between S- and I-type granites in comparison with the classic Lachalan Fold Belt (LFB) granitoids (Fig. 11a; McCulloch and Chappell 1982), which is consistent with mixing of sources with varying compositions (Niu and Batiza 1997). Such isotopic compositions as well as high Sr/Y, La/Yb ratios may be generated by several processes, including (a) classic model of "slab melting" under eclogite facies (Defant and Drummond 1990; Kelemen et al. 2003; Yogodzinski and Kelemen 1998); (b) lower crustal origin (e.g., partial melting of thicken or delaminated lower crust) (Chung et al. 2003; Wang et al. 2005, 2007, 2012); (c) partial melting of remaining part of the subducted ocean crust with terrigenous sediments under amphibolite facies conditions (Mo et al. 2008; Niu 2005; Niu et al. 2013).

The traditional model of partial melting of subducted ocean crust is suitable for explaining the petrogenesis of adakite having typical geochemical characteristics (e.g., high Sr > 400 ppm, Al_2O_3 > 15 wt%), but cannot account for the QCS pluton. Lower crustal origin is also implausible because the $\varepsilon_{Nd}(t)$ (−4.8 to −1.3) of QCS pluton is far above the Nd isotope compositions of mature lower crust. The isotopic compositions with $\varepsilon_{Nd}(t)$ = −4.8 to −1.3 and $\varepsilon_{Hf}(t)$ = −0.7 to +4.0 of QCS pluton indicate significant mantle contribution. Melting of delaminated lower crust in the mantle conditions can be precluded because (1) the QCS pluton has too low MgO (0.16–0.76 wt%) and thus records no interaction between felsic magmas and mantle peridotite and (2) the mechanism of lower crust delamination is still unclear (Niu et al. 2013).

According to the closure time of the North Qilian Ocean (~445 Ma) followed by continental collision (~435–420 Ma) (Song et al. 2013), the ~430 Ma QCS pluton located south of the NQOB is most likely linked with the magmatic response to the collision between the Central Qilian Block and Alashan Block. Partial melting of remaining part of the subducted ocean crust with terrigenous sediments under amphibolite facies conditions offers a better explanation (Mo et al. 2008; Niu

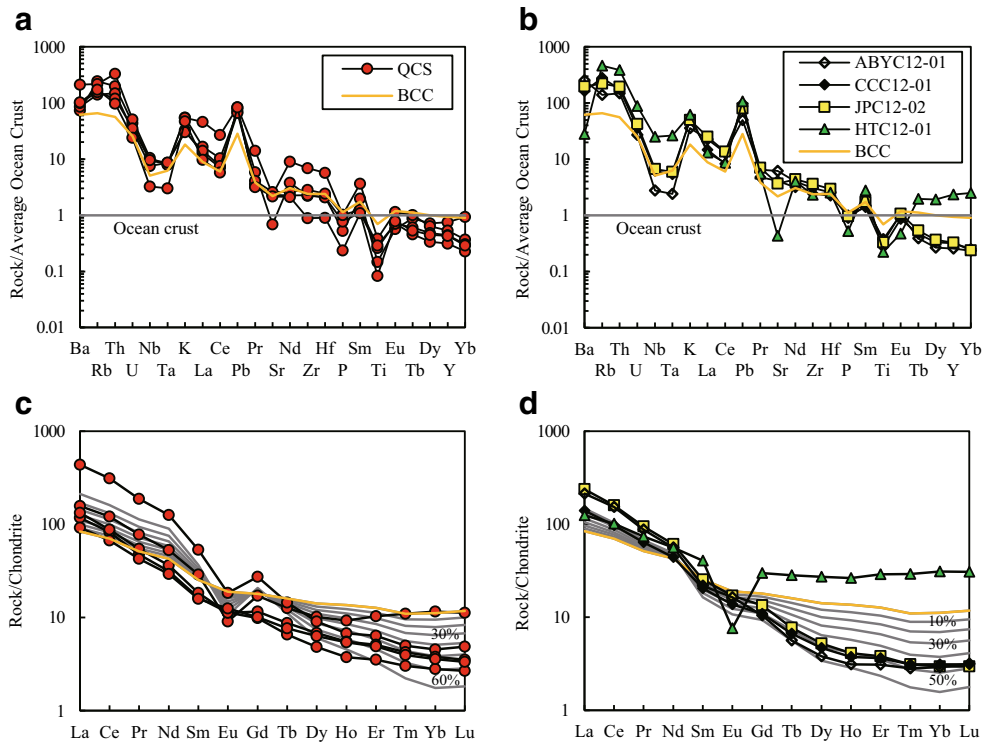

Fig. 7 **a**, **b** Bulk ocean crust normalized (Niu and O'Hara 2003a) trace-element patterns for the Qingchengshan (QCS) pluton and Tongwei (TW) granitoids, respectively. **c**, **d** Chondrite-normalized (Sun and McDonough 1989) rare earth element (REE) patterns for the Qingchengshan pluton and Tongwei granitoids, respectively. Bulk composition of continental crust (BCC) is plotted for comparison. The solid gray lines in **c** are modal curves of fractional crystallization (from the top, the mass fractions of fractional crystallization: 10 %, 20 %, 30 %, 40 %, 50 %, 60 %) with the assemblage of 20 % amphibole +70 % plagioclase +5 % garnet for the Qingchengshan pluton. The solid gray lines in **d** are the same as in **c** with the assemblage of 55 % amphibole +35 % plagioclase +5 % garnet for Tongwei granitoids

2005; Niu et al. 2013). In this model, the retarded underthrusting rate of subducted slab upon collision causes high T/P conditions, making the highly altered ocean crust to melt when intersecting the hydrous basaltic solidus under amphibolite facies conditions and generate andesitic magmas (Mo et al. 2008; Niu et al. 2013).

In our study, we infer that the QCS pluton is the product of the varying extents of fractional crystallization (plagioclase + amphibole + garnet plus minor phase like zircon and other accessary phases) from parental magmas formed as elaborated above. The Sr-Nd-Hf isotopes are also consistent with the modeling (Fig. 11a, b). We use the data of pillow basalts from the North Qilian ophiolite suites representing the remaining part of the ocean crust and of Shaliuhe Gneisses representing terrigenous sediments as the two end-members. The calculation shows that isotopically mantle contribution from ocean crust can reach up to 70 % and is in accord with the melting-induced mixing of two-component source. In addition, we choose the model BCC composition as representing the primitive andesitic magmas parental to the high silicic QCS pluton to evaluate the magma evolution in terms of fractional crystallization. The results show that the primitive magmas with ~50 % fractional crystallization (Fig. 7c) can produce the signature of the QCS pluton.

Petrogenesis of the TW granitoids

Our zircon U-Pb age data show that there are two magmatic emplacement events in the TW area (440.5 ± 2.5 Ma and 229.8 ± 1.5 Ma). It is noteworthy that sample HTC12–01 shows relatively high alkalis (K_2O + Na_2O = 8.41 wt%), low CaO (0.46 wt%), high Nb (39.3 ppm) and Ta (2.95 ppm), and a flat REE pattern with strong negative Sr and Eu anomalies (Sr/Sr* = 0.09, Eu/Eu* = 0.22) (Fig. 7b, d), indicating the possibility of A-type or highly fractionated granites. Using the conventional discrimination indexes for A-type, such as 10,000*Ga/Al, Zr + Nb + Ce + Y et al. (Eby 1992; Whalen et al. 1987), it is hard to distinguish the type of sample HTC12–01 because of only one sample. As is known, the A-type or highly fractionated granites with high LILE and HFSE abundances as well as pronounced negative anomalies (Sr, Eu, Ba, Ti) are largely due to protracted fractional crystallization (e.g., plagioclase, ilmenite) (Anderson et al. 2003; Smith et al. 1999). Isotopically, sample HTC12–01 show extremely high $^{87}Sr/^{86}Sr$ ratio (0.7851), which is consistent with elevated radiogenic ingrowth of ^{87}Sr because of the depletion of Sr (63 ppm) and high Rb/Sr ratio (5.43) (Shao

Table 3 Data of whole-rock Sr-Nd-Hf isotope of the Qingchengshan (QCS) pluton and Tongwei (TW) granitoids

Sample	Age (Ma)	Rb (ppm)	Sr (ppm)	$^{87}Rb/^{86}Sr$	$^{87}Sr/^{86}Sr$(2SD)	$^{87}Sr/^{86}Sr$	Sm (ppm)	Nd (ppm)	$^{147}SM/^{144}Nd$	$^{143}Nd/^{144}Nd$(2SD)	$\varepsilon_{Nd}(t)$	Lu (ppm)	Hf (ppm)	$176_{Lu}/177_{Hf}$	$176_{Hf}/^{177}Hf$ (2SD)	$\varepsilon_{Hf}(t)$
QCS pluton																
QCS12–03	430	181	101	5.056	0.738910(05)	0.707947	4.42	24.8	0.108	0.512152(07)	-4.6	0.29	3.24	0.013	0.282580(06)	-0.7
QCS12–06	430	105	337	0.881	0.712575(05)	0.707181	2.50	14.7	0.103	0.512268(08)	-2.1	0.07	3.22	0.003	0.282632(03)	3.9
QCS12–08	430	162	342	1.336	0.711959(05)	0.703777	8.19	58.8	0.084	0.512256(09)	-1.3	0.12	8.78	0.002	0.282625(06)	4.0
QCS12–10	430	116	379	0.868	0.715322(05)	0.710003	2.81	17.1	0.099	0.512120(10)	-4.8	0.09	3.74	0.003	0.282559(03)	1.2
QCS12–11	430	129	317	1.152	0.714714(06)	0.707656	2.44	13.7	0.108	0.512207(08)	-3.5	0.08	1.39	0.009	0.282612(05)	1.6
TW granitoids																
JPC12–02	230	165	534	0.873	0.710181(06)	0.707325	3.90	28.6	0.082	0.512150(10)	-6.2	0.08	4.52	0.002	0.282509(07)	-4.5
CCC12–01	440	210	599	0.989	0.709842(06)	0.703785	3.12	20.6	0.091	0.512235(10)	-2.1	0.08	3.43	0.003	0.282586(07)	2.2
ABYC12–01	440	105	907	0.326	0.707258(06)	0.705258	3.32	26.2	0.077	0.512139(08)	-3.1	0.08	3.94	0.003	0.282573(05)	1.9
HTC12–01	440	344	63.3	15.363	0.785140(05)	0.691048	6.19	26.1	0.143	0.512237(10)	-4.9	0.78	3.88	0.029	0.282679(08)	-2.0

$^{87}Sr/^{86}Sr_i = (^{87}Sr/^{86}Sr)_{sample} - (^{87}Rb/^{86}Sr)_{sample} * (e^{\lambda t} - 1)$, $\lambda(^{87}Rb) = 1.42 \times 10^{-11}$ $yr.^{-1}$;

$\varepsilon_{Nd}(t) = [(^{143}Nd/^{144}Nd)_{sample}(t) / (^{143}Nd/^{144}Nd)_{CHUR}(t) - 1] * 10{,}000$, where $(^{143}Nd/^{144}Nd)_{CHUR}(t) = (^{143}Nd/^{144}Nd)_{CHUR}(present) - (^{147}Sm/^{144}Nd)_{CHUR}(present) * (e^{\lambda t} - 1)$, $\lambda(^{147}Sm) = 6.54 \times 10^{-12}$ $yr.^{-1}$, The $^{147}Sm/^{144}Nd$ and $^{143}Nd/^{144}Nd$ ratios at the present day are 0.1967 and 0.512638 for chondrite, respectively. t = crystallization age of zircon;

$\varepsilon_{Hf}(t) = [(^{176}Hf/^{177}Hf)_{sample}(t) / (^{176}Hf/^{177}Hf)_{CHUR}(t) - 1] * 10{,}000$, where $(^{176}Hf/^{177}Hf)CHUR(t) = (^{176}Hf/^{177}Hf)_{CHUR}(present) - (^{176}Lu/^{177}Hf)CHUR(present) * (e^{\lambda t} - 1)$, $\lambda(^{176}Lu) = 1.93 \times 10^{-11}$ $yr.^{-1}$, The $^{176}Lu/^{177}Hf$ and $^{176}Hf/^{177}Hf$ ratios at the present day are 0.0332 and 0.282772 for chondrite, respectively. t = crystallization age of zircon

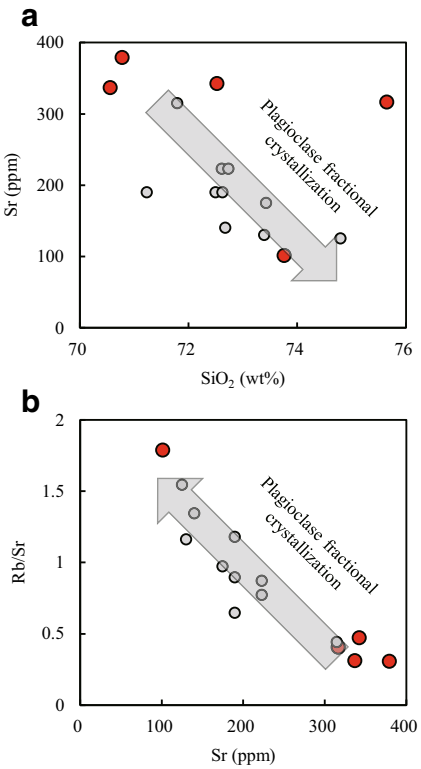

Fig. 8 **a** Sr vs. SiO_2 and **b** Rb/Sr vs. Sr diagrams for the Qingchengshan (QCS) pluton, showing the effect of fractional crystallization of plagioclase. Red circles are our new data, and grey circles are the literature data (Chen et al. 2008)

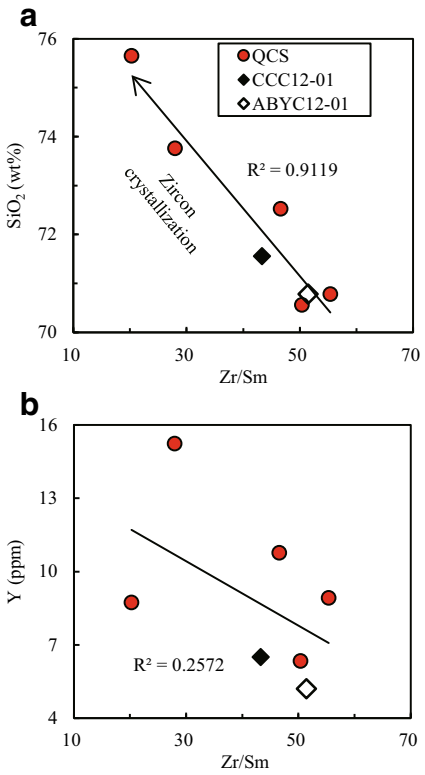

Fig. 9 **a** SiO_2 vs. Zr/Sm diagram for the Qingchengshan pluton (red circles, QCS) and Tongwei (TW) Early Paleozoic granitoids (CCC12–01, ABYC12–01), respectively, showing the effect of zircon crystallization during magma evolution, reflected by rapid decrease of Zr/Sm accompanied by rapid increase of SiO_2. **b** Y vs. Zr/Sm diagram, showing the scattered inverse correlation of heavy rare earth elements (approximated by using Y) with Zr/Sm, indicates that crystallization of zircon is not the cause of the HREE depletion of most of these samples

et al. 2015). The moderate $\varepsilon_{Nd}(t)$ (−4.9) and $\varepsilon_{Hf}(t)$ (−2.0) may point to the significant mantle contribution. However, further study is warranted.

The other ~440 Ma TW granitoids show high SiO_2 (70.8–71.6 wt%), relatively high Sr (599–907 ppm), low Y (5.2–6.5 ppm), low Yb (0.50–0.53), high Sr/Y (92.3–174.4) and La/Yb (62.3–102.1) ratios, negligible Eu anomaly (Eu/Eu* = 0.88–1.02), and relative HREE fractionation ($(Dy/Yb)_N$ = 1.31–1.50). The isotopic compositions show relatively low initial $^{87}Sr/^{86}Sr$ (0.7038 to 0.7053), and high $\varepsilon_{Nd}(t)$ (−2.1 to −3.1) and $\varepsilon_{Hf}(t)$ values (+1.9 to +2.2) (Fig. 11a, b), suggesting mantle contribution to the ~440 Ma TW granitoids through processes elaborated above for the QCS pluton plus amphibole + garnet-dominated fractionation to explain their adakitic features (Fig. 7d; Fig. 10c, d).

As for the ~230 Ma TW granitoids, sample JPC12–02 has high SiO_2 (71.8 wt%), Sr (534 ppm), Sr/Y (80.7) and La/Yb (112.5) values, low Y (6.6 ppm) and Yb (0.50 ppm) contents (Fig. 10c, d), and also shares some geochemical similarities with the ~440 Ma TW granitoids, except for the relatively higher initial $^{87}Sr/^{86}Sr$ (0.7073) and lower $\varepsilon_{Nd}(t)$ (−6.2) and $\varepsilon_{Hf}(t)$ (−4.5) values, implying more crust material involvement in the petrogenesis, which is genetically associated with the Qinling Orogeny (see below).

Tectonic significance of the Qilian Orogenic Belt

There has been a long standing debate on the tectonic evolution of the Qilian Orogenic Belt. Previous studies focus more on the NQOB concerning the continental breakup, seafloor spreading, seafloor subduction and continental collision. The North Qilian Ocean was commonly supposed to open at ~750 Ma as a consequence of breakup of Rodinia supercontinent (Song et al. 2013; Tseng et al. 2006), then subduction occurred some ~200 Myrs later due to the formation of sufficiently cold and thickened lithosphere (Niu et al. 2003b).

In contrast, Huang et al. (2015) suggested that an Early Paleozoic ocean basin (i.e., the Qilian Ocean) could exist between the Qaidam Block and Central Qilian Block in the Neoproterozoic, whereas the back-arc basin (i.e., the North Qilian Ocean) was developed subsequently between the Central Qilian Block and Alashan Block. The recognition of the Qilian Ocean defined above, stretching from the Qaidam Block to West-Qinling Orogenic Belt, has been verified by some studies (Huang et al. 2015; Wu et al. 2006a; Xu et al. 2006; Yang et al. 2015; Zhang et al. 2013). Niu (2014) proposed that back-arc basin originated from within overriding

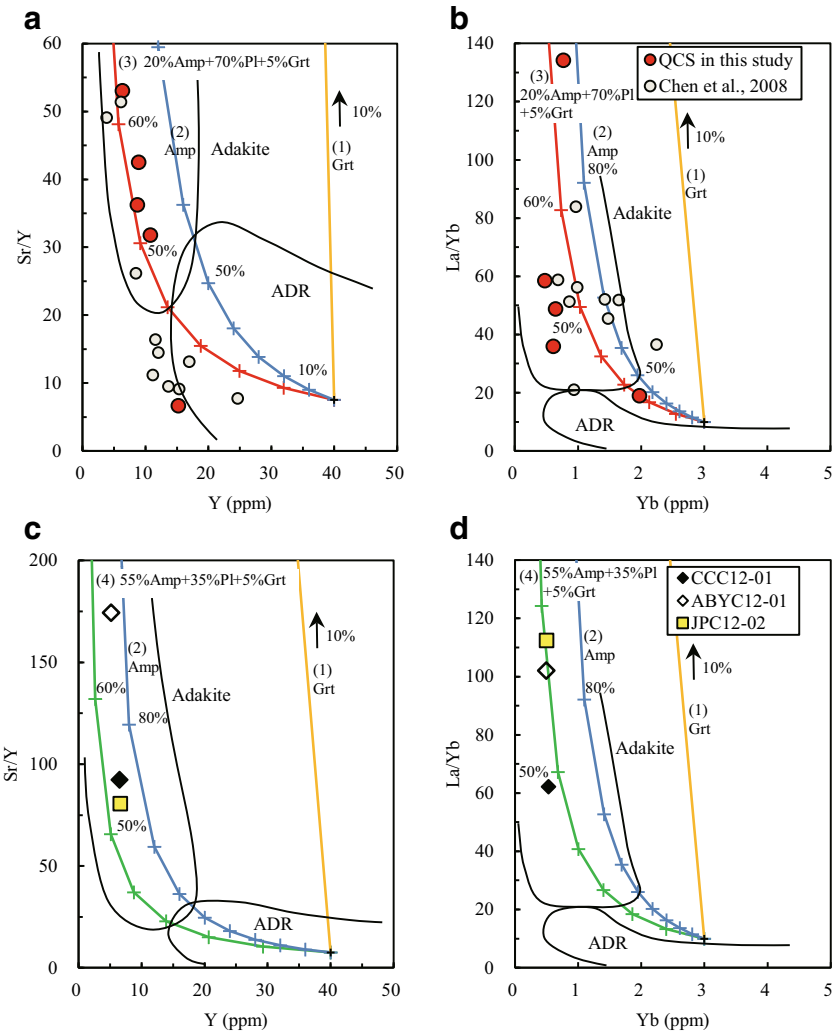

Fig. 10 Plots of **a**, **c** Sr/Y vs. Y and **b**, **d** La/Yb vs. Yb (Castillo 2006, 2012) diagrams that are typically used to distinguish adakite and normal island arc rocks (andesite, dacite and rhyolite, ADR). In **a** and **b**, red circles are our data for the Qingchengshan (QCS) pluton in this study, and grey circles are the literature data (Chen et al. 2008). In **c** and **d**, symbols are the samples from the Tongwei (TW) area (CCC12–01, ABYC12–01, JPC12–02, respectively). All of the data altogether can be explained by the fractional crystallization. Line 1 (garnet fractionation only), and line 2 (amphibole fractionation only) are the same in **a**, **b**, **c** and **d**. Line 3 in **a** and **b**: fractionation by the assemblage of 20 % amphibole (Amp) + 70 % plagioclase (Pl) + 5 % garnet (Grt) for the QCS pluton. Line 4 in **c** and **d**: fractionation by the assemblage of 55 % amphibole +35 % plagioclase +5 % garnet for the Tongwei granitoids. Line 3 and Line 4 explain the data best for the Qingchengshan pluton and Tongwei granitoids, respectively

continental plate in response to the fast trench retreat. Therefore, the northward subduction of the Qilian Ocean seafloor may result in the development of the North Qilian Ocean (back-arc basin) (Huang et al. 2015). The Qilian Ocean was closed at ~460–450 Ma (Huang et al. 2015; Yang et al. 2015), subsequently followed by the closure of the North Qilian Ocean at ~445 Ma (Song et al. 2013). The QCS pluton and TW granitoids are probably generated in such tectonic setting when the North Qilian Ocean was closed.

Currently, an issue under hot debate concerns the subduction tectonic models for the North Qilian Ocean, e.g., northward subduction model (Gehrels et al. 2003a; Song et al. 2013; Yin et al. 2007), southward subduction or bidirectional subduction models (Wu et al. 2006b, 2010; Xia et al. 2003; Xiao et al. 2009). As Fig. 1b shown, synchronous granitoids are widespread in the entire QOB. The single subduction tectonic model cannot account for these granitic magmatic activities in the CQB.

As far as the eastern range of the North Qilian seafloor (i.e., the Qilian Ocean's back-arc basin), its subduction polarity has not yet been recognized for the lack of detailed investigation of geological records and much of the area in eastern section of the CQB are covered by Mesozoic-Cenezoic strata. According to this study, we only emphasize that the North Qilian seafloor may have undergone southward subduction beneath the CQB which is more feasible for explaining the petrogenesis of granitoids represented by the QCS pluton and TW granitods in the eastern section of the CQB, in accord with the closure/collision time. It provides insights into a genuine understanding of the entire QOB evolution.

The significance of ~230 Ma granitoids

Note that sample JPC12–02 from the TW area has an emplacement age of 229.8 ± 1.5 Ma, it could be interpreted as reflecting post-collisional event of the Qilian Orogeny. However, granitoids with such young age are absent elsewhere in the QOB. On the other hand, the coeval granitoid magmatism is abundant in the area adjacent to the Qinling Orogen, especially in the Qingshui area (Fig. 1b). We thus

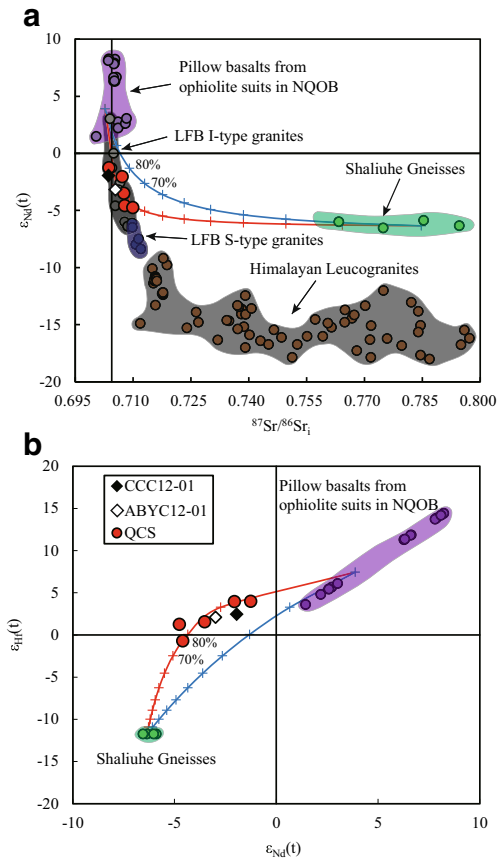

Fig. 11 Plots of **a** $\varepsilon_{Nd}(t)$ vs. $^{87}Sr/^{86}Sr_i$, **b** $\varepsilon_{Hf}(t)$ vs. $\varepsilon_{Nd}(t)$ for the Qingchengshan (QCS) pluton and Tongwei (TW) granitoids (~230 Ma sample not included), showing that they all have distinguishable isotope compositions from LFB (Lachalan Fold Belt) S-type granites and Himalayan leucogranites, and plot along an apparent mixing trend between the North Qilian Orogenic Belt (NQOB) MORB (mid-ocean ridge basalt) and terrestrial sediments (e.g., the Shaliuhe Gneisses). Sr and Nd isotope for the NQOB MORB are data on pillow basalts in the ophilite suites including Yushigou, Jiugequan, Laohushan and Dachadaban (Hou et al. 2006a, 2006b) (we choose the arithmetic average for Sr and Nd as the end-member respectively, Sr: 150 ~ 300 ppm, $^{87}Sr/^{86}Sr$: 0.706115, Nd: 2 ~ 8 ppm, $^{143}Nd/^{144}Nd$: 0.512829, Hf: 2 ppm). Hf isotope for pillow basalts in the NQOB are inferred from Nd isotope data following the equation ($\varepsilon_{Hf} = 1.59\ \varepsilon_{Nd} + 1.28$) by Chauvel et al. (2008). Sr, Nd and Hf isotope data for the Shaliuhe Gneisses are from Chen et al. (2007a, 2007b) (Sr: 50 ~ 100 ppm, $^{87}Sr/^{86}Sr$: 0.858204, Nd: 33 ppm, $^{143}Nd/^{144}Nd$: 0.512148, Hf: 5 ppm, Hf isotope are from the in-situ data zircon of Shaliuhe Gneisses, $^{176}Hf/^{177}Hf$: 0.282180, arithmetic average respectively). Besides, the Sr and Nd isotope data for the Himalayan Leucogranites are from Zhang et al. (2005a); Liao et al. (2006); Zeng et al. (2011), and Guo and Wilson (2012). The Lachlan Fold Belt (LFB) I- and S-type granites are from O'Neil and Chappell (1977); McCulloch and Chappell (1982); Wyborn and Chappell (1983); Gray (1990); Chappell et al. (1991); McCulloch and Woodhead (1993), and Savage et al. (2012)

consider that the granitoids represented by sample JPC12–02 may actually be genetically associated with the Qinling Orogeny (Dong et al. 2011; Wang et al. 2013), which offers an ideal opportunity for future studies on tectonic effects of juxtaposition of younger orogenesis on older orogens.

Conclusions

(1) The Qingchengshan (QCS) pluton was emplaced at ~430–420 Ma, characterized by high SiO_2, high-K calc-alkaline, and high Sr/Y, La/Yb ratios. The diverse granitoids in the Tongwei (TW) area have been identified to include entirely different two magmatic events of 440.5 ± 2.5 Ma and 229.8 ± 1.5 Ma, with high Sr/Y, La/Yb ratios and obvious enrichment of LREEs over HREEs, except for one sample with characteristics of A-type or highly fractionated granites.

(2) The primitive magmas parental to the Qingchengshan (QCS) pluton and the Tongwei (TW) Early Paleozoic granitoids were produced by partial melting of remaining fragments of the subducted ocean crust with terrigenous sediments under amphibolite facies conditions in response to continental collision; such parental magmas have evolved to give rise to the observed compositions through varying extents of fractional crystallization.

(3) The closure of the North Qilian Ocean and the onset of the Central Qilian-Alashan Block collision induced syn-collisional magmatism, generating the ~440–420 Ma Qingchengshan (QCS) pluton and Tongwei (TW) Early Paleozoic granitoids in the eastern section of the Central Qilian Block. The ~230 Ma granitoids in the Tongwei area are genetically associated with the Qinling Orogeny. Further research on granitoids in the Tongwei area will be important for tectonic evolution of the region in a greater context.

Acknowledgments This work was supported by the National Natural Science Foundation of China (NSFC Grants 41130314, 91014003), Chinese Academy of Sciences (Innovation Grant Y42217101L) and grants from regional and local authorities (Shandong Province and City of Qingdao). We thank Pengyuan Guo, Pu Sun, Huixia Cui, Yan Hu, Lei Ye, Jinju Liu and Meng Duan for help with sample preparation. We acknowledge Li Su for the assistance with whole rock major and trace element analysis, and Jinlong Ma with isotope analysis. We also thank editor Yigang Xu for handing this manuscript and two anonymous reviewers for their constructive comments and suggestions.

References

Andersen T (2002) Correction of common lead in U-Pb analyses that do not report ^{204}Pb. Chem Geol 192:59–79

Anderson IC, Frost CD, Frost BR (2003) Petrogenesis of the Red Mountain pluton, Laramie anorthosite complex, Wyoming: implications for the origin of A-type granite. Precambrian Res 124:243–267

Bonin B (2007) A-type granites and related rocks: evolution of a concept, problems and prospects. Lithos 97:1–29

Breiter K, Lamarão CN, Borges RMK, Dall'Agnol R (2014) Chemical characteristics of zircon from A-type granites and comparison to zircon of S-type granites. Lithos 192:208–225

Castillo PR (2006) An overview of adakite petrogenesis. Chin Sci Bull 51:257–268

Castillo PR (2012) Adakite petrogenesis. Lithos 134:304–316

Champion DC, Bultitude RJ (2013) The geochemical and Sr-Nd isotopic characteristics of Paleozoic fractionated S-types granites of north Queensland: Implications for S-type granite petrogenesis. Lithos 162:37–56

Chappell BW (1999) Aluminium saturation in I- and S-type granites and the characterization of fractionated haplogranites. Lithos 46:535–551

Chappell BW, White AJR (1991) Restite enclaves and the restite model. Enclaves and granite petrology. Elsevier Amsterdam 13:479–492

Chappell BW, White AJR (1992) I- and S-type granites in the Lachlan Fold Belt. Geol Soc Am Spec Pap 272:1–26

Chappell BW, Wyborn D (2012) Origin of enclaves in S-type granites of the Lachlan Fold Belt. Lithos 154:235–247

Chappell BW, White AJR, Williams LS (1991) A transverse section through granites of the Lachlan Fold Belt. Second Hutton symposium on granites and related rocks. Australian Bureau of Mineral Resources, Record 22

Chauvel C, Lewin E, Carpentier M, Arndt NT, Marini JC (2008) Role of recycled oceanic basalt and sediment in generating the Hf-Nd mantle array. Nat Geosci 1:64–67

Chen NS, Xia XP, Li XY, Sun M, Xu P, Liu XM, Wang XY, Wang QY (2007a) Timing of magmatism of gneissicgranite plutons along north Qaidam margin and implications for Precambrian crustal accretions: zircon U-Pb dating and Hf isotope evidences. Acta Petrol Sin 23:501–512 (in Chinese with English abstract)

Chen NS, Wang XY, Zhang HF, Sun M, Li XY, Chen Q (2007b) Geochemistry and Nd-Sr-Pb Isotopic Compositions of Granites from Qaidam and Oulongbuluke Micro-Blocks, NW China: constrains on Basement Nature and Tectonic Affinity. Earth Science-J China Univ Geosci 32:7–21 (in Chinese with English abstract)

Chen JL, XY X, Zeng ZX, Xiao L, Wang HL, Wang ZQ, Xiao SW (2008) Geochemical characters and LA-ICP-MS zircon U-Pb dating constrains on the petrogenesis and tectonic setting of the Shichuan intrusion, east segment of the Central Qilian, NW China. Acta Petrol Sin 24:841–854 (in Chinese with English abstract)

Chen YX, Xia XH, Song SG (2012) Petrogenesis of Aoyougou high-silica adakite in the North Qilian orogen, NW China: Evidence for decompression melting of oceanic slab. Chin Sci Bull 57:2289–2301

Chung SL, Liu DY, Ji JQ, Chu MF, Lee HY, Wen DJ, Lo CH, Lee TY, Qian Q, Zhang Q (2003) Adakites from continental collision zones: melting of thickened lower crust beneath southern Tibet. Geology 31:1021–1024

Clemens JD, Stevens G, Farina F (2011) The enigmatic sources of I-type granites: the peritectic connexion. Lithos 126:174–181

Dahlquist JA, Galindo C, Pankhurst RJ, Rapela CW, Alasino PH, Saavedra J, Fanning CM (2007) Magmatic evolution of the Peñón Rosado granite: Petrogenesis of garnet-bearing granitoids. Lithos 95:177–207

Darby BJ, Gehrels G (2006) Detrital zircon reference for the North China block. J Asian Earth Sci 26:637–648

Defant MJ, Drummond MS (1990) Derivation of some modern arc magmas by melting of young subducted lithosphere. Nature 347:662–665

Dong YP, Zhang GW, Neubauer F, Liu XM, Genser J, Hauzenberger C (2011) Tectonic evolution of the Qinling Orogen, China: Review and synthesis. J Asian Earth Sci 41:213–237

Eby GN (1992) Chemical subdivision of the A-type granitoids: petrogenetic and tectonic implications. Geology 20:641–644

Gehrels GE, Yin A, Wang XF (2003a) Magmatic history of the northeastern Tibetan Plateau. J Geophys Res Solid Earth 108. doi:10.1029/2002JB001876

Gehrels GE, Yin A, Wang XF (2003b) Detrital-zircon geochronology of the northeastern Tibetan plateau. Geol Soc Am Bull 115:881–896

Gray CM (1990) A strontium isotopic traverse across the granitic rocks of southeastern Australia: Petrogenetic and tectonic implications. Aust J Earth Sci 37:331–349

Gray CM, Kemp AIS (2009) The two-component model for the genesis of granitic rocks in southeastern Australia-Nature of the metasedimentary-derived and basaltic end members. Lithos 111: 113–124

Guo ZF, Wilson M (2012) The Himalayan leucogranites: Constraints on the nature of their crustal source region and geodynamic setting. Gondwana Res 22:360–376

Guo JJ, Zhang GW, Lu SN, Zhao FQ, Li HK, Zheng JK (1999) Analysis for sedimentary-tectonic setting of the Huangyuan Group in the eastern Mid-Qilian Massif, Qilian Orogenic Belt. Journal of Northwest University 29:343–347 (in Chinese with English abstract)

Hou QY, Zhao ZD, Zhang HF, Zhang BR, Chen YL (2006a) Indian Ocean-MORB-type isotopic signature of Yushigou ophiolite in North Qilian Mountains and its implications. Sci China Ser D 49: 561–572

Hou QY, Zhao ZD, Zhang BR, Zhang HF, Zhang L, Chen YL (2006b) On the boundary of Tethyan tectonic domain on northeastern margin of the Tibetan Plateau. Acta Petrol Sin 22:567–577 (in Chinese with English abstract)

Huang H, Niu YL, Nowell G, Zhao ZD, XH Y, Mo XX (2015) The nature and history of the Qilian Block in the context of the development of the Greater Tibetan Plateau. Gondwana Res 28:209–224

Kelemen PB, Yogodzinski GM, Scholl DW (2003) Along-strike variation in the Aleutian Island Arc: genesis of high Mg# andesite and implications for continental crust. Inside the Subduction Factory Geophys Monogr Ser 138:223–276

Lee CTA, Morton DM (2015) High silica granites: Terminal porosity and crystal settling in shallow magma chambers. Earth Planet Sci Lett 409:23–31

Li XH, Li ZX, Wingate MTD, Chung SL, Liu Y, Lin GC, Li WX (2006) Geochemistry of the 755 Ma Mundine Well dyke swarm, northwestern Australia: part of a Neoproterozoic mantle superplume beneath Rodinia? Precambrian Res 146:1–15

Li JF, Zhang ZC, Han BF (2010) Geochronology and geochemistry of Early Paleozoic granitic plutons from Subei and Shibaocheng areas, the western segment of Central Qilian and their geological implications. Acta Petrol Sin 26:2431–2444 (in Chinese with English abstract)

Liao ZL, Mo XX, Pan GT, Zhu DC, Wang LQ, Zhao ZD, Geng QN, Dong GC (2006) Quzhen peraluminous granite, Tibet: geochemical characteristics and geodynamic significance. Acta Petrol Sin 22: 845–854 (in Chinese with English abstract)

Liu XC, YB W, Gao S, Liu Q, Wang H, Qin ZW, Li QL, Li XH, Gong HJ (2012) First record and timing of UHP metamorphism from zircon in the Xitieshan terrane: implications for the evolution of the entire North Qaidam metamorphic belt. Am Mineral 97:1083–1093

Ludwig KR (2003) A geochronological toolkit for microsoft excel. Isoplot 3:1–70

Ma LF, Qiao XF, Min, LR, Fan BX, Ding XZ (2001) Geological Atlas of China. Geological Publishing House, pp. 90–91

McCulloch MT, Chappell BW (1982) Nd isotopic characteristics of S- and I-type granites. Earth Planet Sci Lett 58:51–64

McCulloch MT, Woodhead JD (1993) Lead isotopic evidence for deep crustal-scale fluid transport during granite petrogenesis. Geochim Cosmochim Acta 57:659–674

Middlemost EAK (1994) Naming materials in the magma/igneous rock system. Earth Sci Rev 37:215–224

Mo XX, Niu YL, Dong GC, Zhao ZD, Hou ZQ, Zhou S, Ke S (2008) Contribution of syncollisional felsic magmatism to continental crust growth: a case study of the Paleogene Linzizong volcanic succession in southern Tibet. Chem Geol 250:49–67

Moyen JF (2009) High Sr/Y and La/Yb ratios: The meaning of the "adakitic signature". Lithos 112:556–574

Niu YL (2005) Generation and evolution of basaltic magmas: Some basic concepts and a new view on the origin of Mesozoic-Cenozoic basaltic volcanism in eastern China. Geol J China Univ 11:9–46

Niu YL (2014) Geological understanding of plate tectonics: basic concepts, illustrations, examples and new perspectives. Global Tectonics and Metallogeny 10:23–46

Niu YL, Batiza R (1997) Trace element evidence from seamounts for recycled oceanic crust in the eastern equatorial Pacific mantle. Earth Planet Sci Lett 148:471–484

Niu YL, O'Hara MJ (2003a) Origin of ocean island basalts: A new perspective from petrology, geochemistry and mineral physics considerations. J Geophys Res 108:2209

Niu YL, O'Hara MJ, Pearce JA (2003b) Initiation of subduction zones as a consequence of lateral compositional buoyancy contrast within the lithosphere: a petrological perspective. J Petrol 44:851–866

Niu YL, Zhao ZD, Zhu DC, Mo XX (2013) Continental collision zones are primary sites for net continental crust growth-a testable hypothesis. Earth Sci Rev 127:96–110

O'Neil JR, Chappell BW (1977) Oxygen and hydrogen isotope relations in the Berridale batholith. J Geol Soc 133:559–571

Pan GT, Xiao QH, SN L, Deng JF, Feng YM, Zhang KX, Zhang ZY, Wang FG, Xing GF, Hao GJ, Feng YF (2009) Subdivision of tectonic units in China. Geol China 36:1–28 (in Chinese with English abstract)

Peccerillo A, Taylor SR (1976) Geochemistry of Eocene Calc-Alkaline Volcanic Rocks from Kastamonu Area, Northern Turkey. Contrib Mineral Petrol 58:63–81

Peng TP, Fan WM, Zhao GC, Peng BX, Xia XP, Mao YS (2015) Petrogenesis of the early Paleozoic strongly peraluminous granites in the Western South China Block and its tectonic implications. J Asian Earth Sci 98:399–420

Qi RR (2012) LA-ICP-MS zircon ages and geological implications for the Bagadeerji granitic plutons in the central Qilian Mountains, Gansu. Sediment Geol Tethyan Geol 32:86–93 (in Chinese with English abstract)

Qian Q, Wang YM, Li HM, Jia XQ, Han S, Zhang Q (1998) Geochemical characteristics and genesis of diorits from Laohushan, Gansu province. Acta Petrol Sin 14:520–528 (in Chinese with English abstract)

René M, Stelling J (2007) Garnet-bearing granite from the Třebíč pluton, Bohemian massif (Czech Republic. Mineral Petrol 91:55–69

Rudnick RL, Gao S (2003) Composition of the continental crust. Treatsite on. Geochemistry 3:1–64

Savage PS, Georg RB, Williams HM, Turner S, Halliday AN, Chappell BW (2012) The silicon isotope composition of granites. Geochim Cosmochim Acta 92:184–202

Shao FL, Niu YL, Regelous M, Zhu DC (2015) Petrogenesis of peralkaline rhyolites in an intra-plate setting: Glass House Mountains, southeast Queensland, Australia. Lithos 216:196–210

Shi RD, Yang JS, CL W, Wooden J (2004) First SHRIMP dating for the formation of the late Sinian Yushigou ophiolite, North Qilian Mountains. Acta Geol Sin 78:649–657 (in Chinese with English abstract)

Smith DR, Noblett J, Wobus RA, Unruh D, Dougalss J, Beane R, Davis C, Goldman S, Kay G, Gustavson B, Saltoun B, Stewart J (1999) Petrolgoy and geochemistry of late-stage intrusions of the A-type, mid-Proterozoic Pikes Peak batholith (Central Colorado, USA): implications for petrogenetic models. Precambrian Res 98:271–305

Song SG, Niu YL, Zhang LF, Wei CJ, Liou JG, Su L (2009a) Tectonic evolution of early Paleozoic HP metamorphic rocks in the North Qilian Mountains, NW China: New perspectives. J Asian Earth Sci 35:334–353

Song SG, Su L, Niu YL, Zhang GB, Zhang LF (2009b) Two types of peridotite in North Qaidam UHPM belt and their tectonic implications for oceanic and continental subduction: A review. J Asian Earth Sci 35:285–297

Song SG, Niu YL, Wei CJ, Li JQ, Su L (2010a) Metamorphism, anatexis, zircon ages and tectonic evolution of the Gongshan block in the northern Indochina continent – An eastern extension of the Lhasa Block. Lithos 120:327–346

Song SG, Su L, Li XH, Zhang GB, Niu YL, Zhang LF (2010b) Tracing the 850 Ma continental flood basalts from a piece of subducted continental crust in the North Qaidam UHPM belt, NW China. Precambrian Res 183:805–816

Song SG, Niu YL, Su L, Xia XH (2013) Tectonic of the North Qilian orogen, NW China. Gondwana Res 23:1378–1401

Song SG, Niu YL, Su L, Zhang C, Zhang LF (2014) Continental orogenesis from ocean subduction, continent collision/subduction, to orogen collapse, and orogen recycling: The example of the North Qaidam UHPM belt, NW China. Earth Sci Rev 129:59–84

Su JP, NG H, Zhang HF, Feng BZ (2004) U-Pb zircon dating and genesis of the Heigouliangzi granitic intrusion in the western segment of the middle Qilian Mountains. Geoscience 18:70–74 (in Chinese with English abstract)

Sun SS, McDonough WF (1989) Chemical and isotopic systematics of oceanic basalts: implications for mantle composition and processes. Geol Soc Lond, Spec Publ 42:313–345

Sylvester PJ (1998) Post-collisional strongly peraluminous granites. Lithos 45:29–44

Taylor J, Stevens G (2010) Selective entrainment of peritectic garnet into S-type granitic magmas: Evidence from Archaean mid-crustal anatectites. Lithos 120:277–292

Thomas JB, Bodnar RJ, Shimizu N, Sinha AK (2002) Determination of zircon/melt trace element partition coefficients from SIMS analysis of melt inclusions in zircon. Geochim Cosmochim Acta 66:2887–2901

Tseng CY, Yang HY, Wan YS, Liu DY, Wen DJ, Lin TC, Tung KA (2006) Finding of Neoproterozoic (775 Ma) magmatism recorded in metamorphic complexes from the North Qilian orogen: evidence from SHRIMP zircon U-Pb dating. Chin Sci Bull 51:963–970

Tung KA, Yang HY, Liu DY, Zhang JX, Yang HJ, Shau YH, Tseng CY (2012) The amphibolite-facies metamorphosed mafic rocks from the Maxianshan area, Qilian block, NW China: A record of early Neoproterozoic arc magmatism. J Asian Earth Sci 46:177–189

Wang Q, McDermott F, JF X, Bellon H, Zhu YT (2005) Cenozoic K-rich adakitic volcanic rocks in the Hohxil area, northern Tibet: lower-crustal melting in an intracontinental setting. Geology 33:465–468

Wang Q, Wyman DA, JF X, Jian P, Zhao ZH, Li CF, Xu W, Ma JL, He B (2007) Early Cretaceous adakitic granites in the Northern Dabie Complex, central China:implications for partial melting and delamination of thickened lower crust. Geochim Cosmochim Acta 71:2609–2636

Wang Q, Li XH, Jia XH, Wyman D, Tang GJ, Li ZX, Ma L, Yang YH, Jiang ZQ, Gou GN (2012) Late Early Cretaceous adakitic granitoids and associated magnesian and potassium-rich mafic enclaves and dikes in the Tunchang-Fengmu area, Hainan Province (South China): Partial melting of lower crust and mantle, and magma hybridization. Chem Geol 328:222–243

Wang XX, Wang T, Zhang CL (2013) Neoproterozoic, Paleozoic, and Mesozoic granitoid magmatism in the Qinling Orogen, China: Constraints on orogenic process. J Asian Earth Sci 72:129–151

Whalen JB, Currie KL, Chappell BW (1987) A-type granites: geochemical characteristics, discrimination and petrogenesis. Contrib Mineral Petrol 95:407–419

Wu CL, Wooden JL, Yang JS, Robinson PT, Zheng LS, Shi RD, Chen SY (2006a) Granitic magmatism in the North Qaidam early Paleozoic ultrahigh-pressure metamorphic belt, Northwest China. Int Geol Rev 48:223–240

Wu CL, Yao SZ, Yang JS, Zeng LS, Chen SY, Li HB, Qi XX, Wooden JL, Mazdab FK (2006b) Double subduction of the Early Paleozoic North Qilian oceanic palt: Evidence from granites in the central

Segment of North Qilian, NW China. Geol China 33:1197–1208 (in Chinese with English abstract)

Wu CL, Xu XY, Gao QM, Li XM, Lei M, Gao YH, Frost RB, Wooden JL (2010) Early Paleozoic granitoid magmatism and tectonic evolution in North Qilian, NW China. Acta Petrol Sin 26:1027–1044 (in Chinese with English abstract)

Wyborn LAI, Chappell BW (1983) Chemistry of the Ordovician and Silurian greywackes of the Snowy Mountains, southeastern Australia: An example of chemical evolution of sediments with time. Chem Geol 39:81–92

Xia XH, Song SG (2010) Forming age and tectono-petrogenises of the Jiugequan ophiolite in the North Qilian Mountain, NW China. Chin Sci Bull 55:1899–1907

Xia LQ, Xia ZC, XY X (2003) Magmagenesis in the Ordovician in back basins of the northern Qilian Mountains, China. Geol Soc Am Bull 115:1510–1522

Xia XH, Song SG, Niu YL (2012) Tholeiite-Boninite terrane in the North Qilian suture zone: Implications for subduction initiation and back-arc basin development. Chem Geol 328:259–277

Xia Y, Xu XS, Zou HB, Liu L (2014) Early Paleozoic crust–mantle interaction and lithosphere delamination in South China Block: Evidence from geochronology, geochemistry, and Sr-Nd-Hf isotopes of granites. Lithos 184–187:416–435

Xiao WJ, Windley BF, Yong Y, Yan Z, Yuan C, Liu CZ, Li JL (2009) Early Paleozoic to Devonian multiple-accretionary model for the Qilian Shan, NW China. J Asian Earth Sci 35:323–333

Xiao YY, Niu YL, Song SG, Davidson J, Liu XM (2013) Elemental responses to subduction-zone metamorphism: Constrains from the North Qilian Mountain, NW China. Lithos 160:55–67

Xu ZQ, Yang JS, CL W, Li HB, Zhang JX, Qi XX, Song SG, Qiu HJ (2006) Timing and mechanism of formation and exhumation of the Northern Qaidam ultrahigh-pressure metamorphic belt. J Asian Earth Sci 28:160–173

Xu YJ, Du YS, Cawood PA, Guo H, Huang H, An ZH (2010a) Detrital zircon record of continental collision: Assembly of the Qilian Orogen. China Sediment Geol 230:35–45

Xu YJ, YS D, Cawood PA, Yang JH (2010b) Provenance record of a foreland basin: Detrital zircon U-Pb ages from Devonian strata in the North Qilian Orogenic Belt, China. Tectonophysics 495:337–347

Xu X, Song SG, Su L, Li ZX, Niu YL, Allen MB (2015) The 600-580 Ma continental rift basalts in North Qilian Shan, northwest China: Links between the Qilian-Qaidam block and SE Australia, and the reconstruction of East Gondwana. Precambrian Res 257:47–64

Yang H, Zhang HF, Luo BJ, Zhang J, Xiong ZL, Guo L, Pan FB (2015) Early Paleozoic intrusive rocks from the eastern Qilian orogen, NE Tibetan Plateau: Petrogenesis and tectonic significance. Lithos 224: 13–31

Yin A, Manning CE, Lovera O, Menold CA, Chen XH, Gehrels GE (2007) Early Paleozoic tectonic and thermomechanical evolution of ultrahigh-pressure (UHP) metamorphic rocks in the Northern Tibetan Plateau, Northwest China. Int Geol Rev 49:681–716

Yogodzinski GM, Kelemen PB (1998) Slab melting in the Aleutians: implication of an ion probe study of clinopyroxene in primitive adakite and basalt. Earth Planet Sci Lett 158:53–65

Yong Y, Xiao WJ, Yuan C, Yan Z, Li JL (2008) Geochronology and geochemistry of Paleo granitic plutons from the eastern Central Qilian and their tectonic implication. Acta Petrol Sin 24:855–866 (in Chinese with English abstract)

Zeng LS, Gao LE, Xie KJ, Zeng JL (2011) Mid-Eocene high Sr/Y granites in the Northern Himalayan Gneiss Domes: Melting thickened lower continental crust. Earth Planet Sci Lett 303:251–266

Zhang Q, Zhou GQ, Wang Y (2003) The distribution of time and space of Chineses ophiolites, and their tectonic setting. Acta Petrol Sin 19:1–8 (in Chinese with English abstract)

Zhang HF, Harris N, Parrish R, Zhang L, Zhao ZD, Li DW (2005a) Geochemistry of North Himalayan leucogranites: regional comparison, petrogenesis and tectonic implications. Earth Science. J China Univ Geosci 30:275–288 (in Chinese with English abstract)

Zhang YJ, Deng YP, Zhang HB (2005b) Genesis and geological characteristics of the granitic batholiths in east Qilian Orogeny. Acta Geological Gansu 14:23–29 (in Chinese with English abstract)

Zhang LF, Wang QJ, Song SG (2009) Lawsonite blueschist in Northern Qilian, NW China: P-T pseudosections and petrologic implications. J Asian Earth Sci 35:354–366

Zhang JX, Mattinson CG, SY Y, Li JP, Meng FC (2010) U-Pb zircon geochronology of coesite-bearing eclogites from the southern Dulan area of the North Qaidam UHP terrane, northwestern China: spatially and temporally extensive UHP metamorphism during continental subduction. J Metamorph Geol 28:955–978

Zhang GB, Zhang LF, Christy AG (2013) From oceanic subduction to continental collision: an overview of HP-UHP metamorphic rocks in the North Qaidam UHP belt, NW China. J Asian Earth Sci 63:98–111

Zhu RZ, Lai SC, Qin JF, Zhao SW (2015) Early-Cretaceous highly fractionated I-type granites from the northern Tengchong block, western Yunnan, SW China: Petrogenesis and tectonic implications. J Asian Earth Sci 100:145–163